isvr Institute of Sound
& Vibration Research

**A Hybrid Model for Wheel/Track Dynamic Interaction
and Noise Generation Due to Wheel Flats**

T.X. Wu and D.J. Thompson

ISVR Technical Memorandum No. 859

January 2001

**University
of Southampton**

SCIENTIFIC PUBLICATIONS BY THE ISVR

Technical Reports are published to promote timely dissemination of research results by ISVR personnel. This medium permits more detailed presentation than is usually acceptable for scientific journals. Responsibility for both the content and any opinions expressed rests entirely with the author(s).

Technical Memoranda are produced to enable the early or preliminary release of information by ISVR personnel where such release is deemed to be appropriate. Information contained in these memoranda may be incomplete, or form part of a continuing programme; this should be borne in mind when using or quoting from these documents.

Contract Reports are produced to record the results of scientific work carried out for sponsors, under contract. The ISVR treats these reports as confidential to sponsors and does not make them available for general circulation. Individual sponsors may, however, authorize subsequent release of material.

UNIVERSITY OF SOUTHAMPTON

INSTITUTE OF SOUND AND VIBRATION RESEARCH

DYNAMICS GROUP

**A Hybrid Model for Wheel/Track Dynamic Interaction
and Noise Generation Due to Wheel Flats**

by

T.X. Wu and D.J. Thompson

ISVR Technical Memorandum No. 859

January 2001

Authorized for issue by
Dr. M.J. Brennan
Group Chairman

ABSTRACT

A numerical model is developed to predict the wheel/rail dynamic interaction occurring due to excitation by wheel flats. A relative displacement excitation is introduced between the wheel and rail that differs from the geometric form of the wheel flat due to the finite curvature of the wheel. To allow for the non-linearity of the contact spring and the possibility of loss of contact between the wheel and the rail, a time-domain model is used to calculate the interaction force. This includes simplified dynamic models of the wheel and the track. In order to predict the consequent noise radiation, the wheel/rail interaction force is transformed into the frequency domain and then converted back to an equivalent roughness spectrum. This spectrum is used as the input to a linear, frequency-domain model of wheel/rail interaction to predict the noise. The noise level due to wheel flat excitation is found to increase with the train speed V at a rate of about $20 \log_{10} V$ whereas rolling noise due to roughness excitation generally increases at about $30 \log_{10} V$. For all speeds up to at least 200 km/h the noise from typical flats exceeds that due to normal levels of roughness. When the wheel load is doubled the predicted impact noise increases by about 3 dB.

CONTENTS

1. INTRODUCTION

When the brakes are applied to a railway wheel, it can sometimes happen that the wheel locks and slides along the rail. The reason for this may be poorly adjusted, defective or frozen brakes or lack of adhesion at the wheel/rail interface, for example due to leaves on the rail head. This sliding causes severe wear of the part of the wheel in contact with the rail, leading to the formation of a 'wheel flat'. Such flats on the wheel may be typically 50 mm long but can extend to over 100 mm long. When the wheels subsequently rotate, these discontinuities on the wheel surface generate large impact forces between the wheel and track. As a consequence, a periodic impact noise is produced in addition to the usual rolling noise, which is more random in character. The large amplitude dynamic forces generated by wheel flats may cause damage to the track, for example resulting in fatigue cracks in the rails or sleepers. The high temperatures reached during sliding, followed by a rapid cooling, lead to the formation of brittle martensite within the steel beneath the wheel flat. As a result, damage to the wheel can also occur, involving cracking and spalling, that is the loss of relatively large pieces of metal [1].

A detailed study of the dynamic interaction between a wheel and the track in response to wheel flats was carried out by Newton and Clark [2], including both predictions and measurements. Their model was composed of (i) the vehicle, consisting of three masses representing the car body, bogie and wheel, plus primary and secondary suspensions, (ii) a non-linear Hertzian contact spring between the wheel and the rail, (iii) the track, consisting of an infinite rail on an elastic foundation. In the field test, instead of using a wheel flat, an equivalent indentation was placed in the railhead. This overcomes the difficulties in locating the position of the flats and their impacts relative to the instrumentation on the track. The indentation was intended to correspond to a rolling wheel with a 'rounded flat', that is one which has undergone further rolling after formation, leading to rounding of the corners and extension of the effective length. Predictions in terms of the ratio of the peak contact force to the static wheel load showed good agreement with the measurements for train speeds up to about 80 km/h. It was shown that the impact force due to the assumed wheel flat increased with increasing train speed and had a peak at about 30 km/h, then decreased slightly up to 60 km/h and increased again thereafter. This observation was consistent with the results of a field experiment reported by the AAR [3]. Although Newton and Clark's work is not related directly to the issue of noise generation, it provides a basis on which to begin a detailed model of impact noise due to wheel flats.

A comprehensive study was carried out by Vér, Ventres and Myles [4] on estimating impact noise generation due to wheel and rail discontinuities. They established the concept of a critical speed, defined as the speed above which loss of contact occurs between the wheel and the rail. They also developed simple formulae for the critical speed, the rail impulse and the speed dependence of the sound power level for five types of discontinuity on the wheel or rail. Remington [5] extended the work of reference [4] and estimated an equivalent roughness spectrum corresponding to wheel flats or rail joints. This allowed the significance of any wheel flat or rail joint to be assessed in terms of its average noise generation capability, in comparison with roughness spectra measured on wheels and rails without significant defects.

The aim of this study is to explore impact noise generation due to wheel flats more precisely and in detail. In order to calculate the wheel/track interaction force, a simplified track model is developed and combined with the wheel through a non-linear Hertzian contact stiffness. Using the combined system of the wheel, contact stiffness and track, dynamic interactions between the wheel and rail are simulated in the time-domain. The results are then analysed in the frequency-domain and the results are compared for different types of wheel flat and different train speeds. The concept of an equivalent roughness spectrum, as in reference [5], is also used in this study. However, here this is not derived from the wheel flat geometry directly, but from the results of the time-domain calculation. Thus it is used as a means of transferring the wheel/rail interaction force into an equivalent roughness input. Using this equivalent roughness input in the TWINS (Track-Wheel Interaction Noise Software [6, 7]) calculation model, the noise radiation from both wheel and track is predicted for excitation by wheel flats having different shapes and sizes.

2. WHEEL FLAT EXCITATION

2.1 Excitation by a new flat

Figure 1 shows a wheel with a newly formed flat rolling on a rail. The size of a wheel flat can be measured by its depth d or its length l. For an idealised flat, without any rounding or wear at its ends, these are related by $d = l^2/8r$ where r is the radius of the wheel. If a rigid wheel with such a flat rolls on a rigid rail without loss of contact, it will pivot about the front corner of the flat until the flat is horizontal, and then pivot about the rear corner until it can again roll on the round part of the wheel, see Figure 1(b).
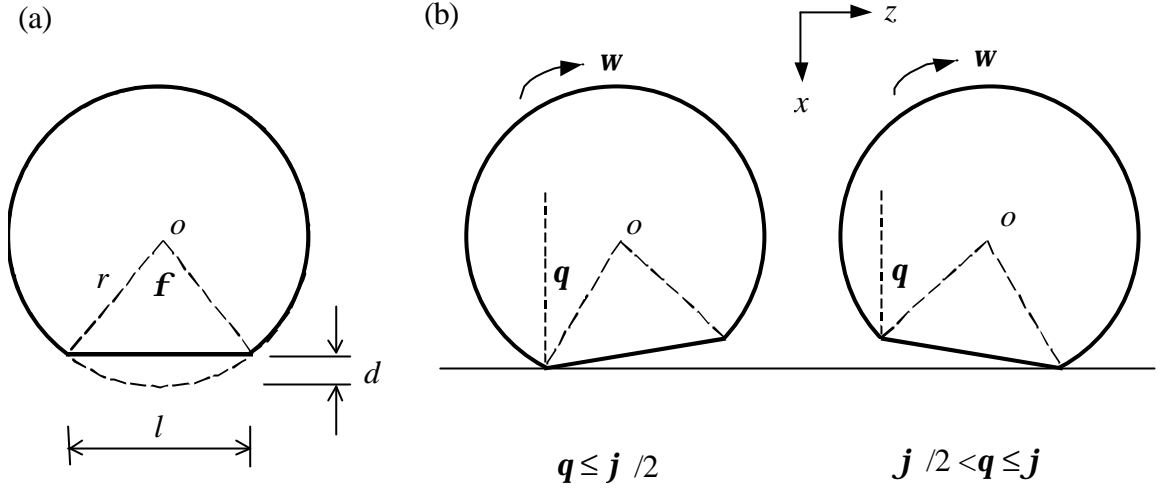
Figure 1. Rolling of a wheel with an idealised flat.

From geometrical considerations, the vertical movement of the wheel centre, x_0 (positive downwards) is given by

$$x_0 = \begin{cases} r(1-\cos q), & 0 \le q \le j/2, \\ r[1-\cos(j-q)], & j/2 < q \le j, \end{cases} \tag{1}$$

where $j = 2\cos^{-1}[(r-d)/r]$ is the angle subtended by the flat at the wheel centre and is dependent on the wheel radius and flat size. x_0 will be termed the wheel centre 'trajectory'.

As the flat depth d is much smaller than the wheel radius r, the angle j is small and equation (1) can be approximately expressed in terms of the longitudinal distance, $z = rq$,

$$x_0 \approx \begin{cases} z^2/2r, & 0 \le z \le l/2, \\ (l-z)^2/2r, & l/2 < z \le l. \end{cases} \tag{2}$$

Clearly x_0 differs from the shape of the wheel flat itself, due to the finite size of the wheel. Figure 2(a) shows the shape of the wheel with a new flat as well as that of a round wheel, with the vertical scale exaggerated. The shape of the flat can be expressed as a profile height, x_p, which is the difference between the two curves in Figure 2(a). This is given by

$$x_p(z) \approx \frac{1}{2r}\left(\frac{l^2}{4} - \left(z - \frac{l}{2}\right)^2\right) = d - \frac{1}{2r}\left(z - \frac{l}{2}\right)^2, \qquad 0 \le z \le l \tag{3}$$

This is the profile that would be measured by a probe with a small radius of curvature. The profile, x_p, and the wheel centre trajectory, x_0, are compared in Figure 2(b) from which it can be seen that the lengths and depths are both equal but that the trajectory, x_0, has a quite different shape to the flat geometry, x_p.
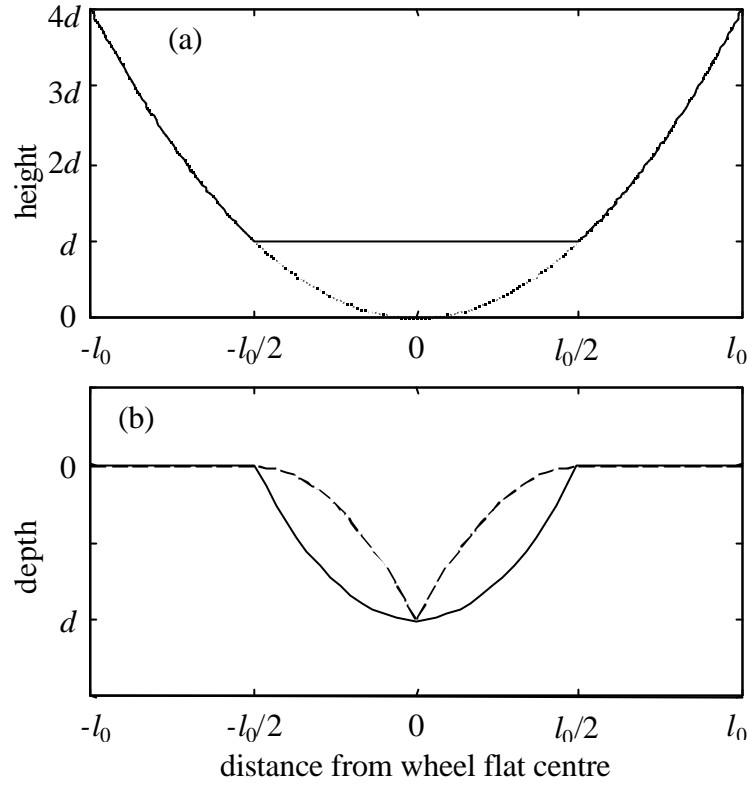
−3−

Figure 2. Wheel flat geometry for new flat of length l_0, (a) wheel geometry, - - - - with flat, ✕✕✕✕round wheel, (b) with wheel curvature removed. - - - - profile depth, - - - wheel centre trajectory.

As neither the track nor the wheel are rigid, the actual motion of the wheel centre is much more complicated than that described in equation (2). However, equation (2) can be used as the *relative displacement* excitation between a flexible track and wheel in the same way that the roughness is used as the input for rolling noise calculations [7]. If the train speed is high, loss of contact may occur, and an impact between the wheel and rail occurs when the wheel hits the rail again. Loss of contact is allowed for within the contact spring (see Section 3) and does not affect the form of the input defined by equation (2).

2.2 Excitation by a rounded flat

In practice, due to continued running of the wheel after formation of the flat, the profile becomes rounded at the corners of the flat, whereas the central part will remain unchanged. The overall length of the rounded flat, l, will be greater than that for a new flat of the same depth, l_0. Figure 3(a) shows three such rounded flats with the same depth, d, but different lengths, l.
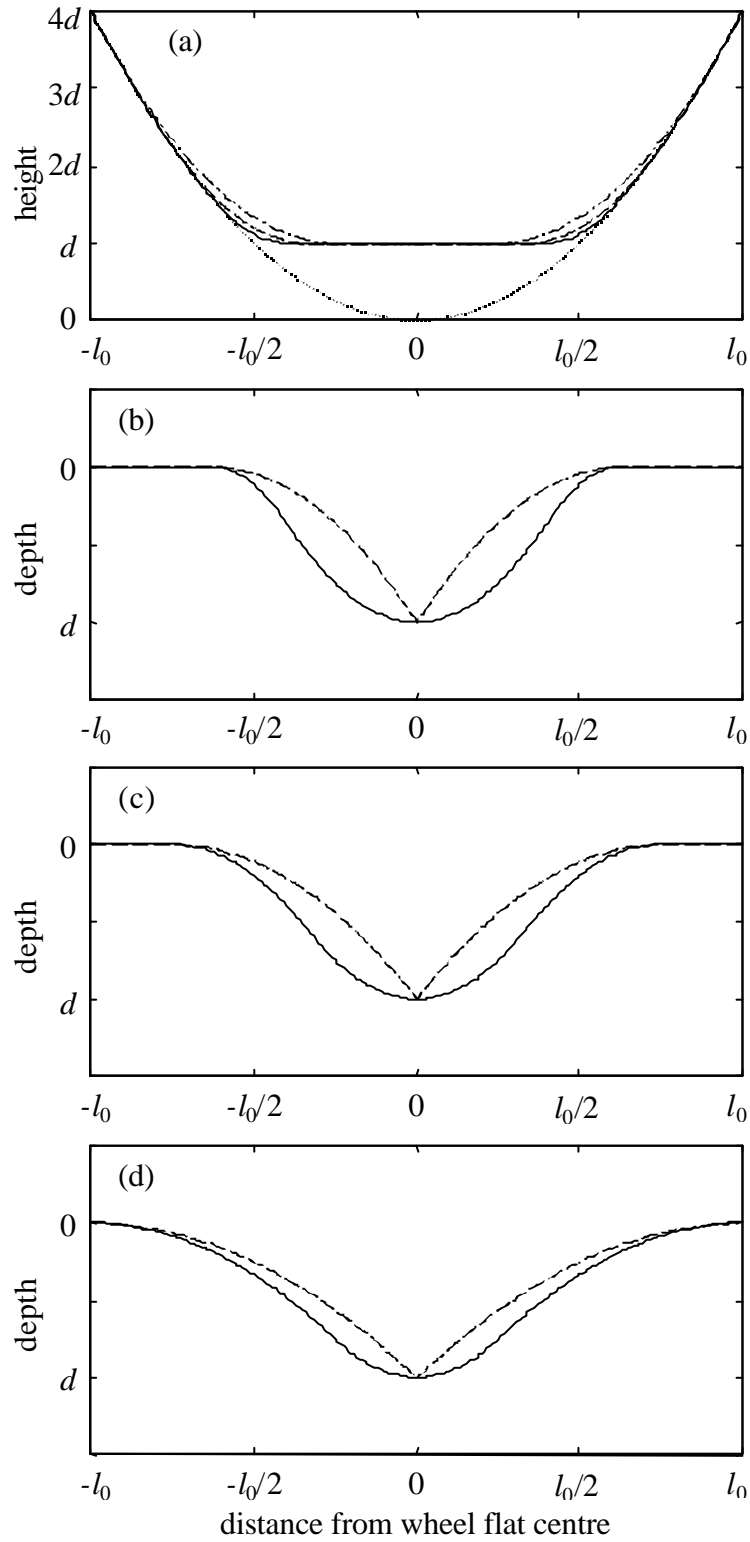
Figure 3. *Wheel flat geometry for rounded flats (a) wheel shape for various rounded flats, - - - - total length $l = 5l_0/4$, - - - total length $l = 3l_0/2$, - ×- ×total length $l = 2l_0$, with l_0 the length of the equivalent new flat, (b) rounded flat, total length $l = 5l_0/4$, - - - - profile depth (with wheel curvature removed), - - - wheel centre trajectory, (c) rounded flat, total length $l = 3l_0/2$, key as (b), (d) rounded flat, total length $l = 2l_0$, key as (b).*

If it can be assumed that these rounded corners can be represented by a *quadratic* function with smooth transitions, it is shown in Appendix A that the wheel centre trajectory will be described by

$$x_0 \approx \begin{cases} 4d \, (z/l)^2, & 0 \le z \le l/2, \\ 4d \, ((l-z)/l)^2, & l/2 < z \le l. \end{cases} \tag{4}$$

where l is the length of the rounded flat and d is the depth (which is no longer simply related to the length l). This expression clearly satisfies the requirements that $x_0 = 0$ at $z = 0$ and at $z = l$, and $x_0 = d$ and $z = l/2$. In fact, equation (2) is a special case of equation (4) for the case $d = l^2/8r$. Thus equation (4) can be used for both new flats and rounded flats of the type considered here.

Figure 3 shows the flat profile and the wheel centre trajectory for three idealised rounded flats. It can be seen that the wheel centre trajectories are identical to that in Figure 2 except that they are stretched in the z direction.

In practice, a rounded flat will differ in geometry from the idealised case considered here. However, in the absence of measured data, equation (4) will be used in this study to represent the dynamic excitation to the wheel/rail system. For measured flat profiles a numerical procedure can be employed to determine the wheel centre trajectory.

2.3 Excitation by equivalent rounded flat on the rail

It is also possible to assume that the wheel is perfectly round but that the railhead has an equivalent indentation. This was used in the field tests in reference [2], where the following irregularity profile was introduced onto the railhead for the tests,

$$x_p(z) = \frac{d}{2}(1 - \cos 2\boldsymbol{p}\,\frac{z}{l}), \tag{5}$$

where the depth d was 2.15 mm and the overall length l was 150 mm. When a round wheel rolls over the curve described above, its centre trajectory can be given as

$$x_0(z_0) = x_p(z) + r(1 - \cos \boldsymbol{q}), \tag{6a}$$

$$z_0 = z + r \sin \boldsymbol{q}, \tag{6b}$$

where

$$\boldsymbol{q} \approx \tan \boldsymbol{q} = x'_r(z) = \frac{\boldsymbol{p}d}{l}\sin 2\boldsymbol{p}\,\frac{z}{l}. \tag{6c}$$

These expressions are derived using the same method as given in Appendix A for the rounded flat of the last section.

Figure 4 shows both the irregularity curve described by equation (5) and the wheel centre trajectory calculated using equations (6) for a wheel[1] of radius 0.46 m. From this it is seen that the size of the wheel modifies the effective input provided by the irregularity (flat) in a similar way to that found above. However, the dimensions of the irregularity in reference [2] are such that the wheel can roll over the whole of the rail, i.e. if converted to an equivalent 'flat' it would not be flat at its centre but slightly convex. As a result, the contact point does not jump along the rail, as before, and the trajectory is slightly rounded at its trough, unlike those in Figure 3.
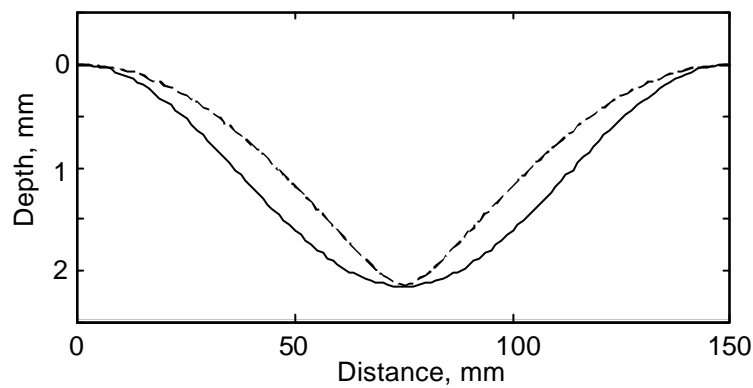

Figure 4.   Wheel flat geometry from equation (5), r = 460 mm, d = 2.15 mm and l = 150 mm. ¾¾ irregularity on the railhead, - - - wheel centre trajectory.

3. WHEEL/RAIL INTERACTION MODEL

3.1 Wheel/track interaction model

The wheel/track interaction model is shown schematically in Figure 5. The vehicle system is simplified to a static load W and a wheel. This is because the vibration frequency of interest here is within the audio-frequency range, for example $50 - 5000$ Hz, whilst the natural frequency of the vehicle-suspension system is only a few Hertz, and thus the low frequency vibration of the vehicle body and bogie is effectively isolated from the high frequency vibration of the wheel and track. The track model is composed of an infinite Timoshenko beam on a continuous spring-mass-spring foundation representing the rail pads, sleepers and ballast respectively. Damping is introduced by adding loss factors to the pad and ballast stiffness. The wheel and rail are

---

[1] The vehicle used in reference [2] was a COV-AB 2-axle covered freight wagon. The wheel radius of such a vehicle is 0.47 m new (37 inches diameter). The value of 0.46 m therefore represents a partially worn wheel.

connected via a Hertzian contact stiffness which is non-linear; the contact force is proportional to the elastic contact deflection to the power 3/2, provided that loss of contact does not occur.
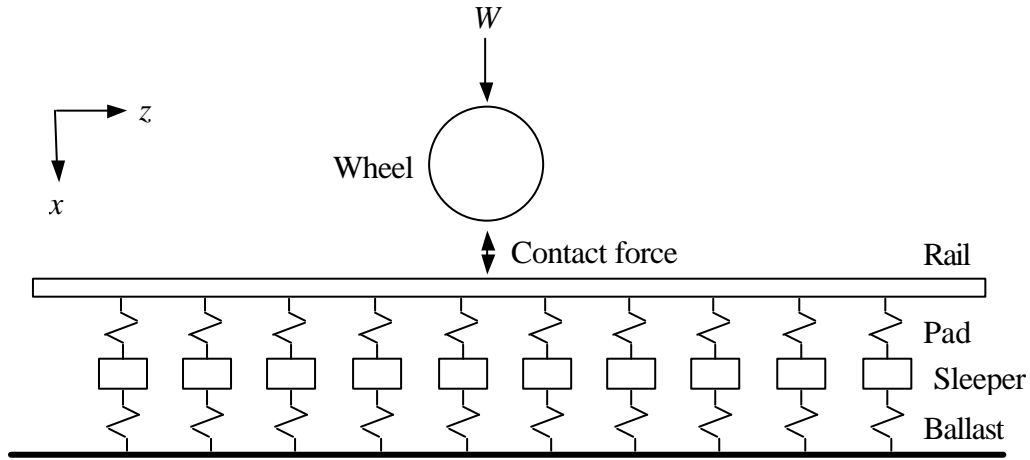

Figure 5. Wheel/track interaction model.

As the train speed is much lower than the speed of flexural wave propagation in the rail in the frequency region of interest, a moving irregularity model can be used to simulate the wheel/rail interaction [8]. In such a model the wheel remains stationary on the rail and an irregularity is effectively moved at the train speed between the wheel and rail as a relative displacement excitation. The source of vibration here is a wheel flat and the moving irregularity is represented by the 'wheel centre trajectory', as calculated above.

Since the contact stiffness is non-linear and loss of contact may occur, it is necessary to calculate the wheel/rail dynamic interaction in the time-domain. To do so, the main difficulties arise from the track model, because it is required that calculations are performed over an infinite spatial extent. On the other hand, the track model is considered to be linear and its dynamic properties are needed only at the contact position for the calculation of wheel/rail interactions. Thus it is possible to develop an equivalent but much simpler system with only a single input (force) and a single output (displacement) to replace the track model represented in Figure 5. If this linear system has the same frequency response function (both amplitude and phase) as the track, it can be mathematically substituted for the track [9].

3.2 Simplified track model

The vibration behaviour of the continuously supported Timoshenko beam model on the spring-mass-spring layers is similar to a two degree of freedom system at low frequencies,

because here the motion of the beam is strongly dependent on the foundation stiffness. At high frequencies, however, the beam vibration is coupled much more weakly to the foundation and it shows a free-beam like behaviour. In terms of the point receptance, such a track model can be approximated by a system with the following transfer (frequency response) function:

$$H(s) = \frac{X(s)}{F(s)} = \frac{b_1 s^3 + b_2 s^2 + b_3 s + b_4}{s^4 + a_1 s^3 + a_2 s^2 + a_3 s + a_4},$$

(7)

where $X(s)$ and $F(s)$ are the Laplace transforms of the displacement (output) and force (input) at the contact position respectively. Constant coefficients a_i and b_i are determined by minimising the differences between $H(i\boldsymbol{w})$ and the point receptance of the track in the frequency region of interest.

For a track with the parameters described in Table 1, its point receptance is shown in Figure 6 (solid line). Also shown in Figure 6 is the frequency response function of equation (7) (dotted line). It can be seen that $H(i\boldsymbol{w})$ is in good agreement with the point receptance of the infinite track model in the frequency region $50 - 5000$ Hz. Thus the simple model described by equation (7) can be used to replace the infinite beam model in terms of its point receptance to calculate the dynamic interaction between the wheel and track.

Table 1. Parameters describing the track vertical dynamics.

|		
Young's modulus of rail, N/m^2	E	2.1×10^{11}
Shear modulus of rail, N/m^2	G	0.77×10^{11}
Density of rail, kg/m^3	$\boldsymbol{r}$	7850
Loss factor of rail	$\boldsymbol{h}_r$	0.02
Cross-section area of rail, m^2	A	7.69×10^{-3}
Second moment of area, m^4	I	30.55×10^{-6}
Shear coefficient	$\boldsymbol{k}$	0.4
Pad stiffness per unit length of rail, N/m^2	k_p	583×10^6
Pad loss factor	$\boldsymbol{h}_p$	0.25
Sleeper mass (half, per unit length of rail), kg/m	m_s	270
Ballast stiffness per unit length of rail, N/m^2	k_b	83.3×10^6
Ballast loss factor	$\boldsymbol{h}_b$	1.0
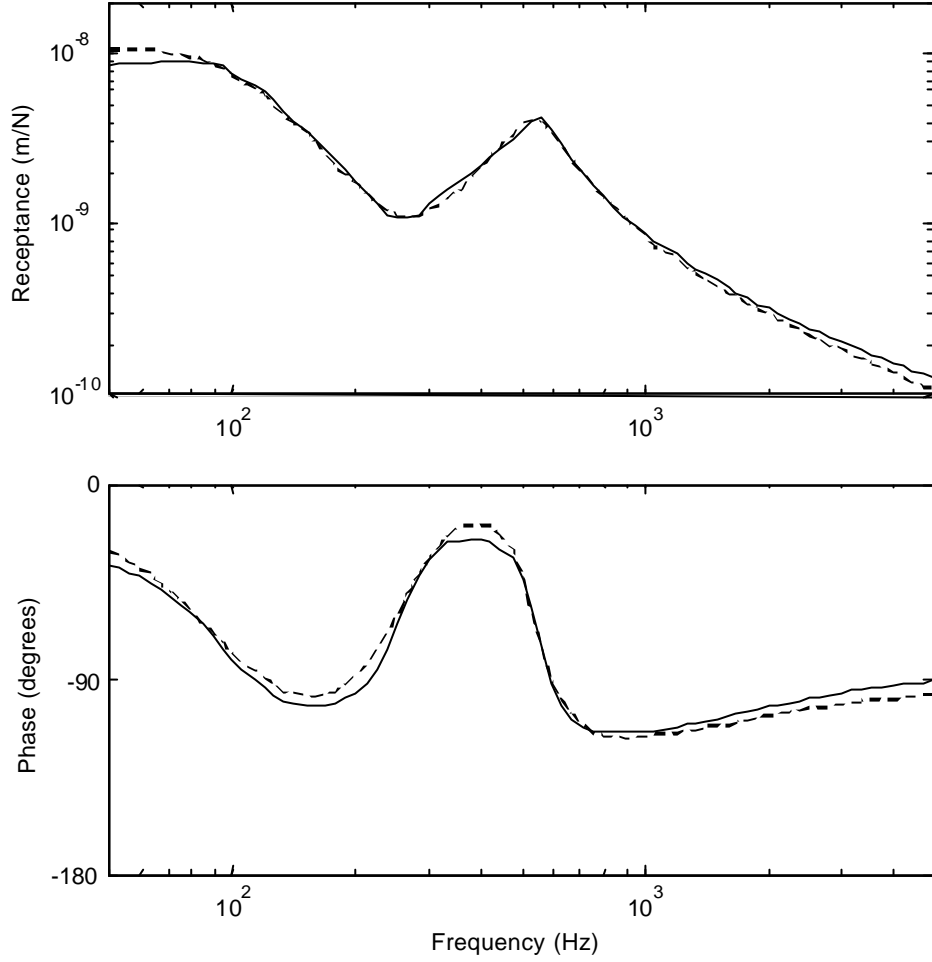
Figure 6. *Amplitude and phase of the track frequency response function. ¾¾ Point receptance of the continuously supported track model, ✖✖✖frequency response function of the simplified track model, which is calculated using equation (7), where $b_1 = 3.28 \times 10^{-6}$, $b_2 = 1.87 \times 10^{-2}$, $b_3 = 23.6$, $b_4 = 3.97 \times 10^{4}$, $a_1 = 1.77 \times 10^{3}$, $a_2 = 1.26 \times 10^{7}$, $a_3 = 7.87 \times 10^{9}$, $a_4 = 3.93 \times 10^{12}$.*

3.3 Simplified wheel model

The simplified wheel model is composed of two masses, a spring and a dashpot, see Figure 7. The larger mass M_w is the unsprung mass of the wheel. The spring k_w is used to match the main trough around 460 Hz found in the measurements of the wheel receptance at the contact point. The damping c_w is used to reduce the sharpness of this trough. The small mass m_w is added, so that the wheel can be coupled with the track via a non-linear contact stiffness without mathematical difficulties. As this mass is very small, its influence on the wheel dynamic properties is negligible for frequencies up to 10 kHz.
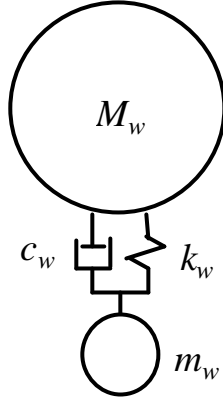
Figure 7. Simple wheel model. $M_w = 600$ kg, $m_w = 3$ kg, $k_w = 5$ GN/m, $c_w = 2\mathbf{z}\sqrt{k_w M_w}$ and $\mathbf{z} = 0.025$.

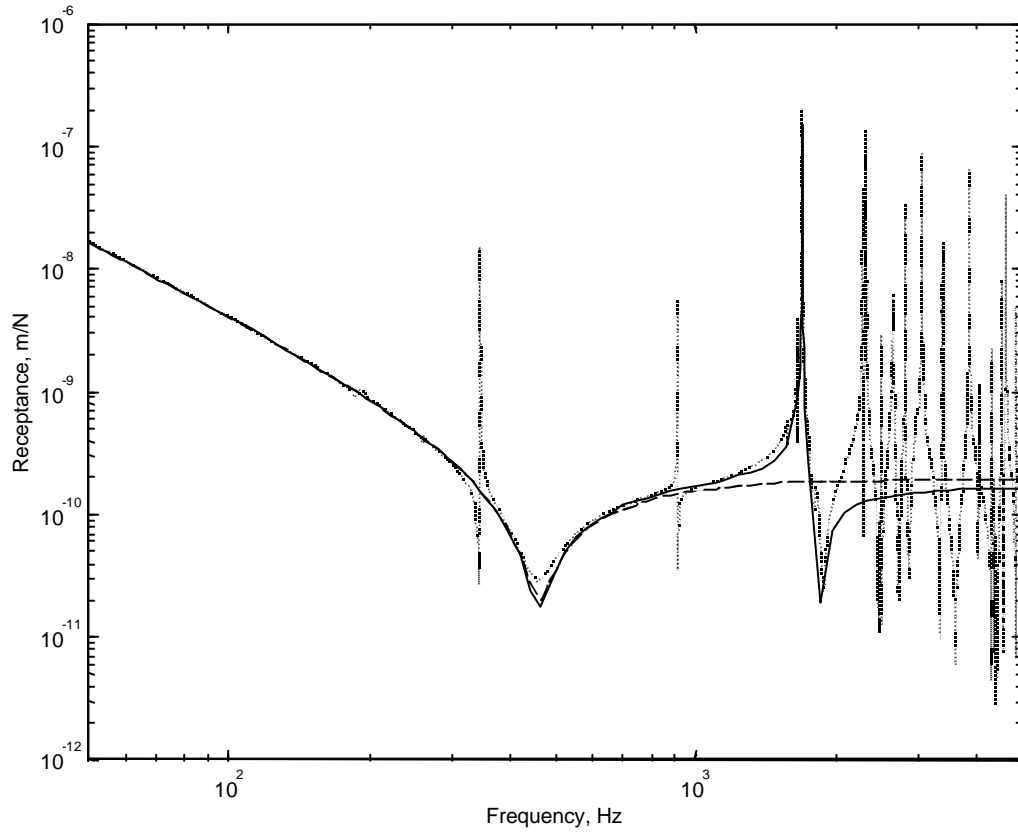*Figure 8. Wheel receptance for UIC 920 mm freight wheel. - - - simple model of Fig. 7, ▨▨▨full model from finite element mesh, ¾¾ simplified modal model (Section 5.3).*

The deficiency of this simplified wheel model is that the high frequency modes of the wheel above 1 kHz are neglected. Figure 8 shows the wheel receptances of the simplified model and of a full model based on a finite element prediction. It is seen that there are many resonant peaks and troughs in the full model which are not present in the simplified model. The effects on the wheel/rail interaction of the high frequency wheel modes, which are ignored due to the use of the

−11−

simplified model, may be considered using a special treatment, the use of an equivalent roughness excitation. This will be discussed later in Section 5.

4. SIMULATION OF WHEEL/RAIL INTERACTION DUE TO WHEEL FLATS

4.1 Equation of motion for wheel/rail interaction

The equivalent track model given by equations (7) can be expressed in the time-domain using a state-space form. Coupling the simplified wheel model with the track model through a Hertzian contact force, the equations of motion for the wheel/rail interaction can be written in the state-space form. The equations for the wheel are

$$
\begin{aligned}
\dot{x}_1 &= x_2, \\
\dot{x}_2 &= [W - k_w(x_1 - x_3) - c_w(x_2 - x_4)]/M_w, \\
\dot{x}_3 &= x_4, \\
\dot{x}_4 &= [k_w(x_1 - x_3) - c_w(x_2 - x_4) - f]/m_w
\end{aligned}
\tag{8a}
$$

where x_3 is the wheel displacement (the displacement of the small mass m_w), x_1 is the displacement of the upper mass, W is the static load from the vehicle weight, and f is the non-linear wheel/rail interaction force. The rail motion is given by the state-space form of equations (7):

$$
\begin{bmatrix} \dot{x}_5 \\ \dot{x}_6 \\ \dot{x}_7 \\ \dot{x}_8 \end{bmatrix} = \begin{bmatrix} -a_1 & 1 & 0 & 0 \\ -a_2 & 0 & 1 & 0 \\ -a_3 & 0 & 0 & 1 \\ -a_4 & 0 & 0 & 0 \end{bmatrix} \begin{bmatrix} x_5 \\ x_6 \\ x_7 \\ x_8 \end{bmatrix} + \begin{bmatrix} b_1 \\ b_2 \\ b_3 \\ b_4 \end{bmatrix} f,
\tag{8b}
$$

where x_5 is the rail displacement, and the interaction force is given by

$$
f = \begin{cases} C_H(x_3 - x_5 - x_0)^{3/2}, & x_3 - x_5 - x_0 > 0, \\ 0, & x_3 - x_5 - x_0 \leq 0, \end{cases}
\tag{8c}
$$

where x_0 is the relative displacement excitation due to the wheel flats, described for example in equation (4) for the idealised newly formed or rounded flats. Here x_0 is a function of time, and so becomes dependent on the train speed.

Simulations of the wheel/rail dynamic interaction have been carried out in the time-domain using the fourth order Runge-Kutta method with a constant time step.

4.2 Comparison with measured impact force

Firstly, predictions from equations (8) are compared with the test results from reference [2] in terms of the ratio of the peak force to the static load, to validate the above model. This is shown in Figure 9. The calculation parameters are chosen here according to reference [2] and the relative displacement excitation, x_0, is calculated using equations (6). The track parameters are those in Table 1.
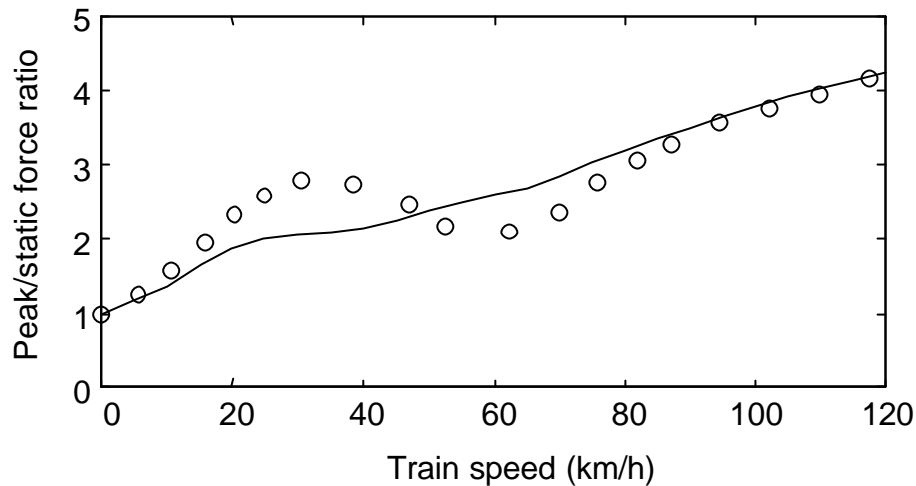

Figure 9.   Comparison of the predictions with the field test results. Parameters used for predictions are from reference [2], with a railhead indentation input, d = 2.15 mm, l = 150 mm. ¾¾ Predictions, o o o test results [2].

It can be seen that the predictions are very close to the test results for train speeds $0 - 15$ km/h and $80 - 120$ km/h, whereas between 20 and 40 km/h the contact forces are underestimated by up to about 30%. In general, however, the predictions using the simplified model are actually better than those in reference [2] which were based on three types of theoretical model for the track (an Euler beam on an elastic foundation, a Timoshenko beam on an elastic foundation and a discretely supported Euler beam).

It should be noted that the track parameters quoted in reference [2] differ slightly from those used here. In particular, the pad stiffness is about half the value used here. Moreover, although the actual irregularity that was ground into the rail followed closely the form given in equation (5), some detail differences were present.

4.3 Impact force for wheel flats

Since the model of equations (8) is much simpler than the beam model it replaces, detailed simulations can be performed readily for different wheel flats and train speeds. Example results

are presented in Figures 10 and 11 in terms of the wheel/rail interaction force, and the wheel and rail displacements at the contact position. Here the static load from the vehicle weight is chosen as $W = 100$ kN, the wheel radius $r = 0.46$ m, the wheel mass $M_w = 600$ kg and the Hertzian constant $C_H = 93.7$ GN/m$^{3/2}$. The parameters for the track are shown in Table 1.
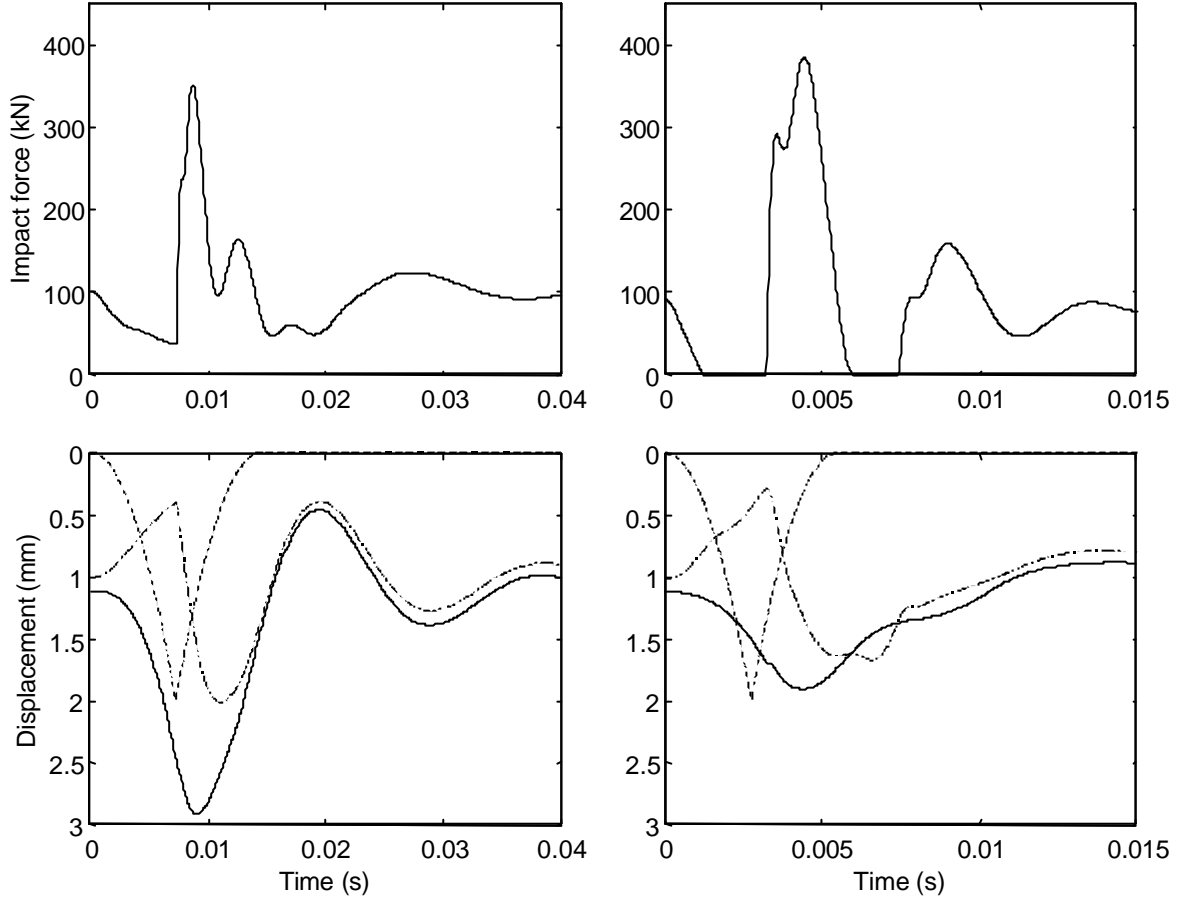

Figure 10. Wheel/rail interaction and displacements of wheel and rail due to 2 mm rounded wheel flat. (a) At train speed 30 km/h, (b) at 80 km/h, ¾¾ wheel displacement, - ×- ×rail displacement, ✕✕✕relative displacement excitation.

Figure 10 shows the wheel/rail interaction due to a rounded wheel flat with depth $d = 2$ mm and length $l = 121$ mm. At a train speed of 30 km/h (Figure 10(a)), partial unloading occurs and the maximum contact force is about 3.5 times as large as the static load. When the indentation (relative displacement input due to the wheel flat) appears between the wheel and rail (the sign convention adopted is positive for an indentation and for downwards displacements), the wheel falls and the rail rises. Since the wheel and rail cannot immediately follow the indentation due to their inertia, the contact force is therefore partly unloaded. If the train speed is low, the static load is sufficient to maintain contact between the wheel and rail. After the relative displacement input

–14–

reaches its maximum, the contact force increases rapidly until it reaches its peak. At this stage the relative displacement input decreases and the rail is forced to move downwards, but the wheel still keeps falling for a while due to its large inertia.

At a speed of 80 km/h (Figure 10(b)) loss of contact occurs twice. The first impact occurs at about 3.5 ms when the wheel hits the rail again after the first loss of contact. Here the force rises dramatically and the ratio of the peak force to static load is greater than 4. Since the momentum of the wheel and rail are changed dramatically by the large impulse during this first impact, the wheel and rail are forced to move apart from each other and a second loss of contact occurs at about 7.5 ms. However, the second impact is much smaller than the first one.
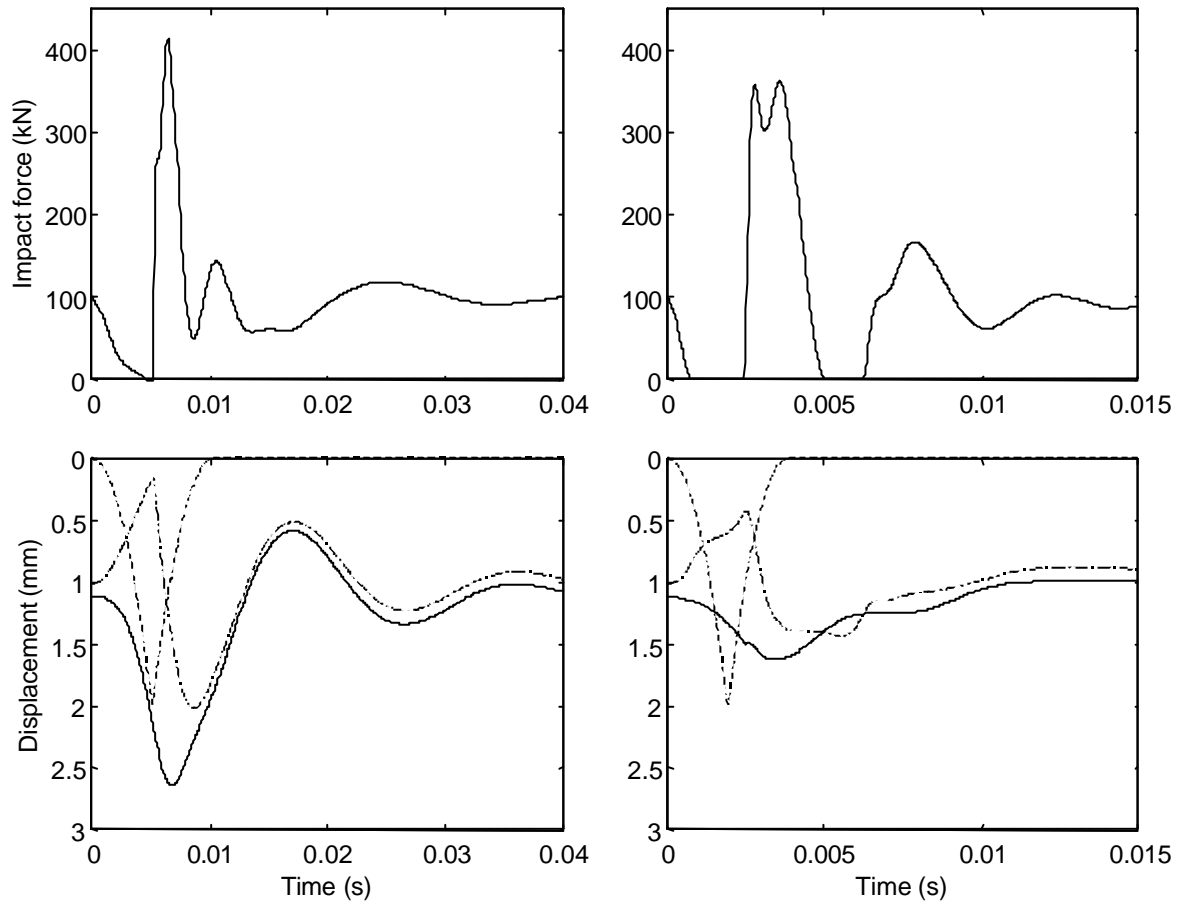

Figure 11. Wheel/rail interaction and displacements of wheel and rail due to 2 mm newly formed wheel flat. (a) At train speed 30 km/h, (b) at 80 km/h, ¾¾ wheel displacement, - ×- ×rail displacement, ⬤⬤⬤relative displacement excitation.

Figure 11 shows the results due to a newly formed wheel flat with depth $d = 2$ mm and length $l = 86$ mm. At a speed of 30 km/h (Figure 11(a)) slight loss of contact between the wheel and rail occurs. The maximum impact force here is larger than that for the rounded flat at 30 km/h, see Figure 10(a). This is because the duration of the displacement excitation here is shorter than for the rounded flat, while the peak values are the same for both, thus the accelerations of the wheel and rail are higher, and therefore the impact force is larger. At a speed of 80 km/h (Figure 11(b)), however, the impact force peak is smaller than that for the rounded flat. This is also because of the shorter duration of the relative displacement input. When the wheel contacts the rail again after loss of contact, the remaining displacement excitation is shorter and smaller compared with the rounded flat case, see Figures 10(b) and 11(b). As a result the impact force here is smaller.

The wheel/rail interaction force is periodic, repeating once every wheel revolution. In order to convert it to the frequency domain, a discrete Fourier transform is obtained of the force calculated for a whole wheel revolution. For example at a speed of 30 km/h the fundamental frequency of this discrete spectrum is 2.88 Hz; at 120 km/h it is 11.5 Hz. These results are then converted to one-third octave band spectra in order to facilitate comparison between the results at different speeds. Figure 12 shows the force spectra produced from new and rounded flats of depth 2 mm at four speeds.
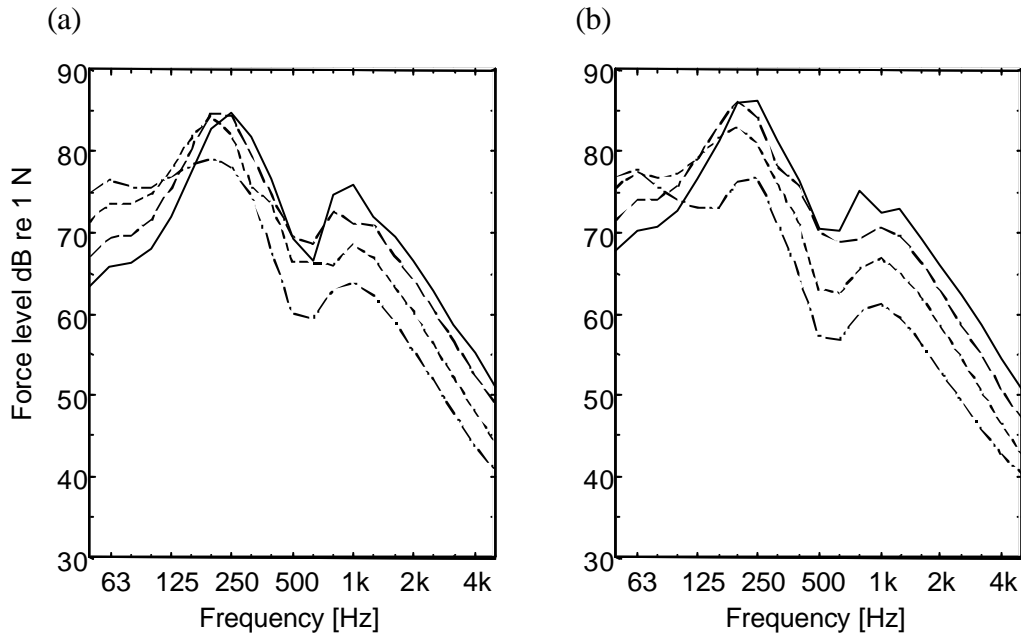

(a) (b)

Figure 12. One-third octave spectra of the impact force caused by wheel flats at different train speeds. (a) Due to 2 mm newly formed flats, (b) due to 2 mm rounded flats. ¾¾ At 120 km/h, - - - at 80 km/h, ⨯⨯⨯at 50 km/h, - ×- ×at 30 km/h.

It can be seen that the main components of the impact force are in the region 100 to 1000 Hz. Below about 100 Hz the force spectrum decreases slightly with increasing speed. At high frequencies the level increases considerably as the speed increases due to the shortening of the impact force pulse. This is more noticeable in the case of the rounded flat (Figure 12(b)).

These results illustrate that, in general, the impact force caused by wheel flats is related to both the shape of the flat and the train speed. The peak forces at different train speeds are presented in Figure 13 for the wheel flats of different types and size. Two flat types are considered here, based on equation (4): a rounded one ($l = 121$ mm for $d = 2$ mm) and the newly formed one ($l = 86$ mm for $d = 2$ mm). Two flat depths are chosen for each type: $d = 1$ mm and $d = 2$ mm. At low speeds the peak forces increase with increasing speed and they are larger for the newly formed flats than for the rounded flats. For a given flat depth the peak forces are the same for both types of flat considered but these maxima are reached at higher speed for the rounded flats. This is a consequence of the fact that equation (4) is used in both cases. At higher speeds they decrease to slightly lower levels. At high speeds the peak forces are smaller for the newly formed flats than for the rounded flats. It can also be observed from Figure 13 that the deeper the wheel flats are, the larger are the impact forces.
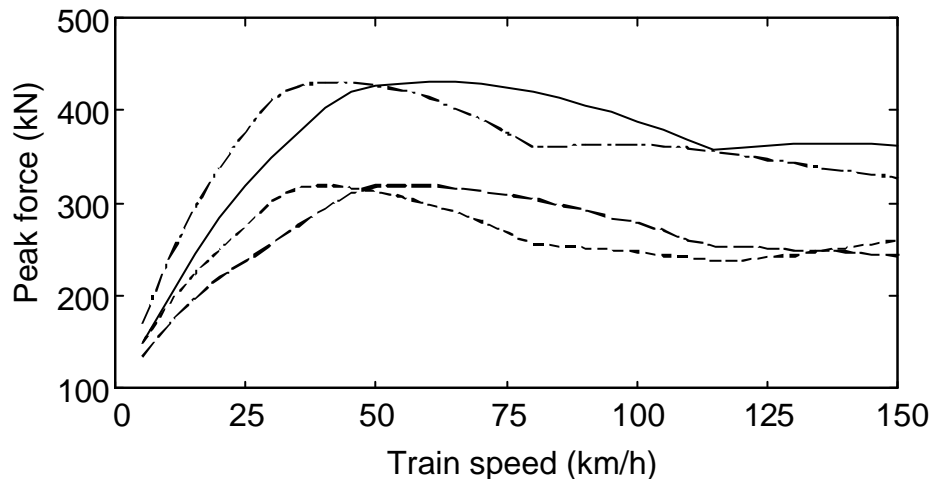

Figure 13.   Peak impact force caused by different wheel flats. ¾¾ due to 2 mm rounded flat, - - - 1 mm rounded flat, - ×- ×2 mm newly formed flat, ⨯⨯⨯1 mm newly formed flat.

5. A HYBRID METHOD FOR PREDICTING VIBRATION AND NOISE FROM WHEEL FLATS

5.1 Background

The modelling so far has concentrated on the response of the wheel/rail system at the contact zone to the excitation from a wheel flat. The vibration so generated will be transmitted in the form of structural waves through the track which will radiate noise; it will also excite modes of vibration of the wheel which will radiate noise. Suitable models for the prediction of structural response and sound radiation of tracks and wheels are available within the TWINS (Track-Wheel Interaction Noise Software) model [6, 7] which is used for predicting rolling noise due to random roughness excitation. These models operate in the frequency domain and are normally used with a linear interaction model.

In order to predict the noise radiation due to wheel flat excitation, a model is required that takes account of the modal behaviour of the wheel. It is known from studies of rolling noise that the wheel modes containing a significant radial component of motion at the contact zone dominate the noise radiation of the wheel/rail system in the frequency region above about 2 kHz [10].

The inclusion of all such modes in the time-domain model of wheel/rail interaction has not been considered in the present work, since there are many such modes and these have very light damping (loss factors around 10^{-4}). Consequently they have a large time constant and numerical integration of the response becomes difficult.

The proposed method of overcoming this difficulty is referred to here as a hybrid method and is summarised in Figure 14. The interaction force from a wheel flat is calculated first in the time domain using the simplified wheel model described above. Then, after conversion of this result to the frequency domain, this is applied as an excitation to a more complete model of the wheel and rail. However, this hybrid approach requires some additional precautions, described below.
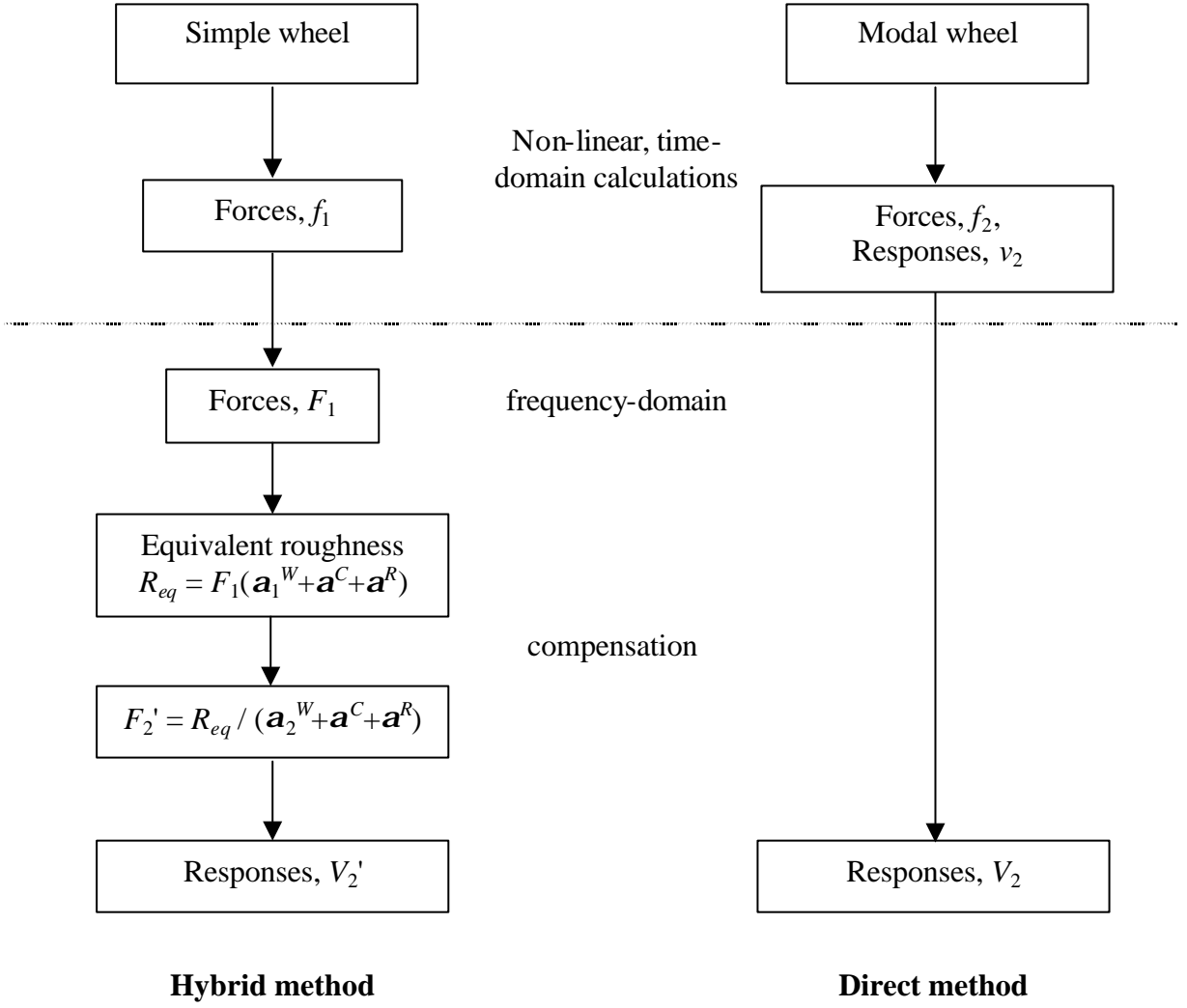
Simple wheel → **Forces, f_1**

Modal wheel → **Forces, f_2, Responses, v_2**

Non-linear, time-domain calculations

Forces, F_1

frequency-domain

Equivalent roughness
$$R_{eq} = F_1(\boldsymbol{a}_1^{W} + \boldsymbol{a}^{C} + \boldsymbol{a}^{R})$$

compensation

$$F_2{}' = R_{eq} / (\boldsymbol{a}_2^{W} + \boldsymbol{a}^{C} + \boldsymbol{a}^{R})$$

Responses, $V_2{}'$

Responses, V_2

Hybrid method   **Direct method**

Figure 14. An overview of the hybrid method.

5.2 Contact force and equivalent roughness

The main obstacle to using the method outlined above is that it is known from rolling noise studies that the interaction force depends on the wheel and track dynamic properties as well as the roughness input. For a roughness excitation $R(\boldsymbol{w})$, at angular frequency $\boldsymbol{w}$, and considering only interaction in the vertical direction, the interaction force $F(\boldsymbol{w})$ is given by

$$F(\boldsymbol{w}) = -\frac{R(\boldsymbol{w})}{\boldsymbol{a}^{W}(\boldsymbol{w}) + \boldsymbol{a}^{C}(\boldsymbol{w}) + \boldsymbol{a}^{R}(\boldsymbol{w})} \tag{9}$$

where $\boldsymbol{a}^{W}$, $\boldsymbol{a}^{C}$ and $\boldsymbol{a}^{R}$ are the receptances of the wheel, the contact spring and the rail respectively.

At a wheel resonance, the denominator is large due to a sharp peak in the wheel receptance. Consequently the contact force has a sharp minimum at this frequency, and in the wheel response this partially cancels the peak in the wheel receptance. Although the wheel response spectrum during rolling has peaks corresponding to each resonance of the wheel, their amplitude and bandwidth are consistent with a much higher level of damping than is present in the free wheel. This is sometimes referred to as 'rolling damping' [11].

For interaction in multiple degrees of freedom, the situation is less straight-forward, with the force component in the lateral direction cancelling that in the vertical direction rather a simple dip occurring in the force amplitude at wheel resonances. Nevertheless it remains true that, in the vicinity of wheel resonances, the force spectrum depends strongly on the wheel receptance. The use of a force spectrum calculated from a different wheel model would prevent this matching of the force spectrum with the wheel receptance and would produce wheel vibration estimates that are too high, since they effectively ignore the rolling damping.

To illustrate this, the results of some example studies are given in Appendix B.

5.3 Simulations using a simplified modal wheel model

From the discussion in Section 5.2 it follows that the interaction force estimated using a simple mass/spring model for the wheel, such as Figure 7, cannot be applied to a modal model of the wheel to calculate its response. Instead, it is possible to convert the interaction force back to an 'equivalent roughness' spectrum – the roughness (relative displacement) input between the wheel and rail models that would produce the same force spectrum *if the contact spring were linear*. This is obtained by calculating the Fourier transform of the interaction force and using equation (9) in reverse to derive an equivalent roughness spectrum:

$$R(\boldsymbol{w}) = -F(\boldsymbol{w})\big(\boldsymbol{a}^{W}(\boldsymbol{w}) + \boldsymbol{a}^{C}(\boldsymbol{w}) + \boldsymbol{a}^{R}(\boldsymbol{w})\big) \qquad (10)$$

The question that remains is whether the same equivalent roughness would be obtained if the high frequency modal behaviour of the wheel were taken into account. In other words, are high frequency oscillations in the contact force induced by wheel modes independent of the non-linear effects that occur essentially at low frequencies? (Note that the duration of the wheel flat events in Figures 10 and 11 is of the order of 10 to 20 ms).

To demonstrate that this is in fact the case, a model is considered for the wheel containing a single lightly damped mode; this comprises three masses, two springs and two dampers, as shown

in Figure 15. This system is referred to as a simplified modal wheel. Its receptance is shown as the solid line in Figure 8. Comparing this result with that from the full finite element wheel model, it can be seen that good agreement is found up to about 2 kHz, including the first main, lightly damped, resonance at high frequency (1688 Hz).
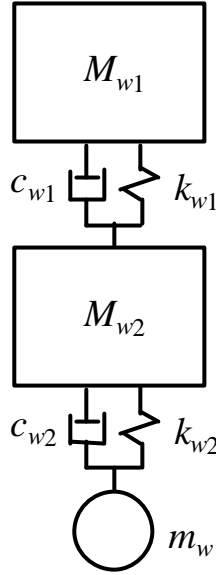

Figure 15. Simplified modal wheel model. $M_{w1} = 400$ kg, $M_{w2} = 200$ kg, $m_w = 3$ kg, $k_{w1} = 15$ GN/m, $k_{w2} = 5.92$ GN/m, and respective damper rates $c_{w1} = 0.245$ kNs/m and $c_{w2} = 54.4$ kNs/m.

Two methods are now used to determine the response of this wheel to a wheel flat input and their results compared. The first is direct integration in the time domain using the Runge Kutta method, indicated by the right-hand side of Figure 14. The second is the proposed hybrid method, indicated by the left-hand side of Figure 14. In this, the wheel-rail contact force is calculated in the time domain using the mass-spring wheel model (Figure 7); this force is transformed into the frequency domain and then converted back to an equivalent roughness spectrum using equation (10); this roughness is then applied in the frequency domain as the excitation of a wheel-rail system containing the simplified modal wheel model of Figure 15.

Figure 16(a) shows an example result for a 2 mm new flat, a wheel load of 50 kN and a train speed of 80 km/h. The graph shows the wheel velocity spectrum at the contact point. The result from the two methods (direct and hybrid) agree closely. Also shown is the result obtained for the mass/spring wheel model, showing the extent of the correction applied by the hybrid method. This correction is small below 1 kHz, but up to 12 dB in the band containing the resonance.
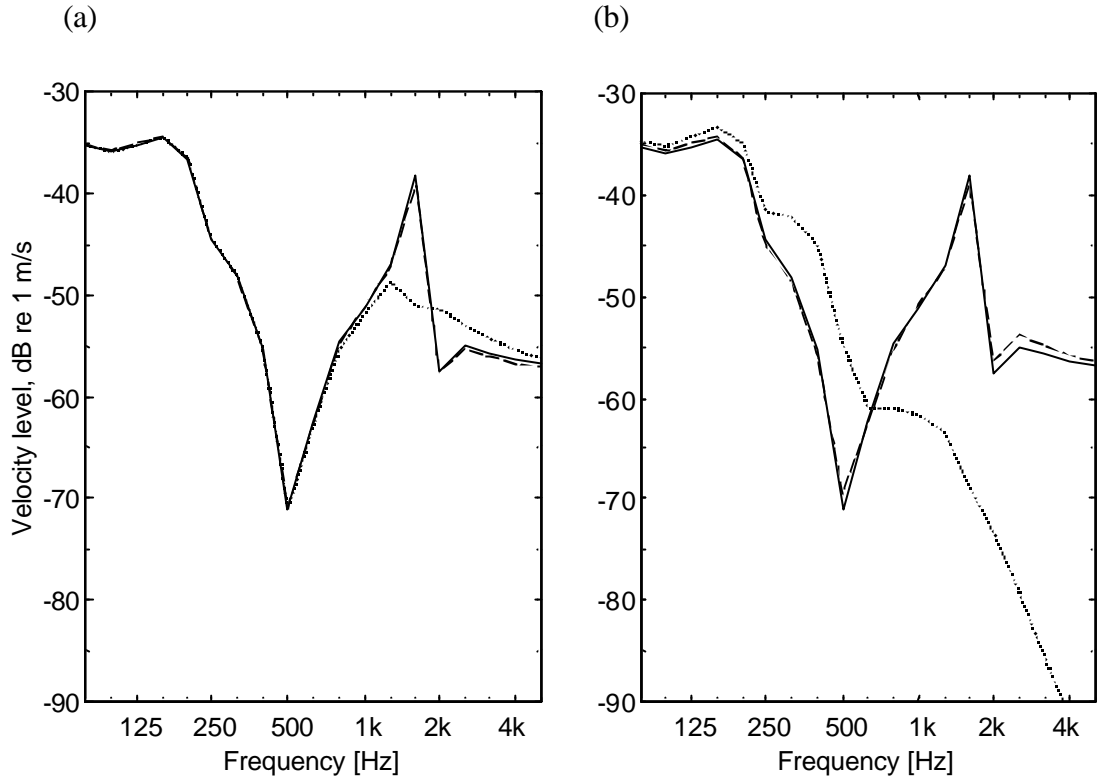
Figure 16. Wheel velocity spectrum at the contact point for a 2 mm new flat, a wheel load of 50 kN and a train speed of 80 km/h for the simplified modal wheel. (a) based on mass/spring wheel (Fig. 7), (b) based on unsprung mass only. ¾¾ from the direct method, - - - from the hybrid method, ✖✖✖for the mass/spring wheel before correction is applied.

If, instead of the mass/spring wheel model of Figure 7, the wheel is represented in the hybrid approach by a single mass, the error is greater and covers a wider frequency range. This can be seen from the results shown in Figure 16(b).

These results have been repeated for loads of 25, 50 and 100 kN, for speeds of 40, 80 and 160 km/h and for new wheel flats of 1 mm and 2 mm depth. The differences found are shown in Figure 17 for the hybrid method based on the mass/spring wheel model. These differences represent the error introduced by using the hybrid method. This error is very small for frequencies less than 1600 Hz. The band containing the lightly damped resonance is the only band containing significant error – the error in this band is found to be less than 2 dB in every case. For a full wheel model containing many modes, it can be expected that a similar level of agreement will be found in the whole of the modal region, i.e. above 1.6 kHz.
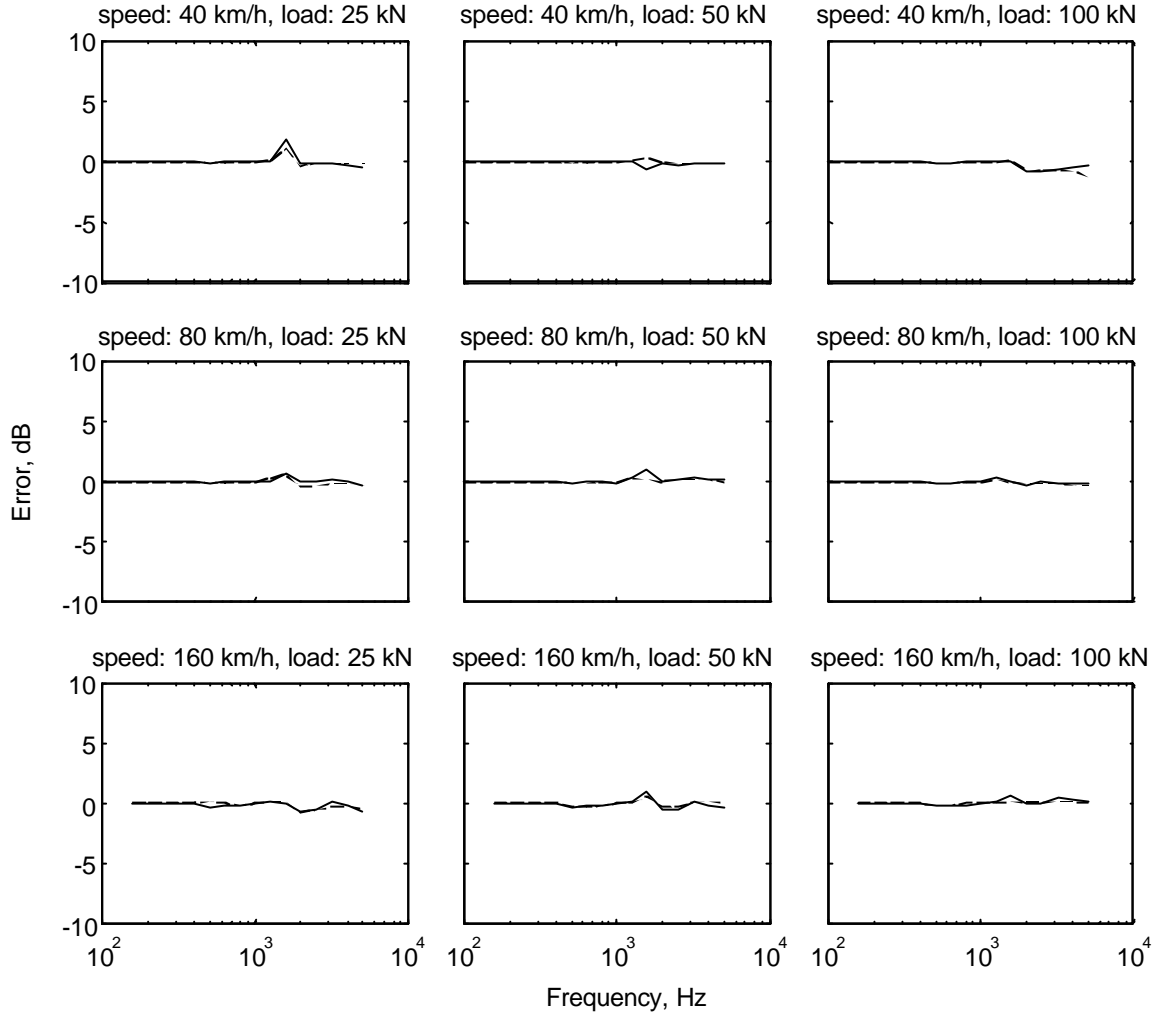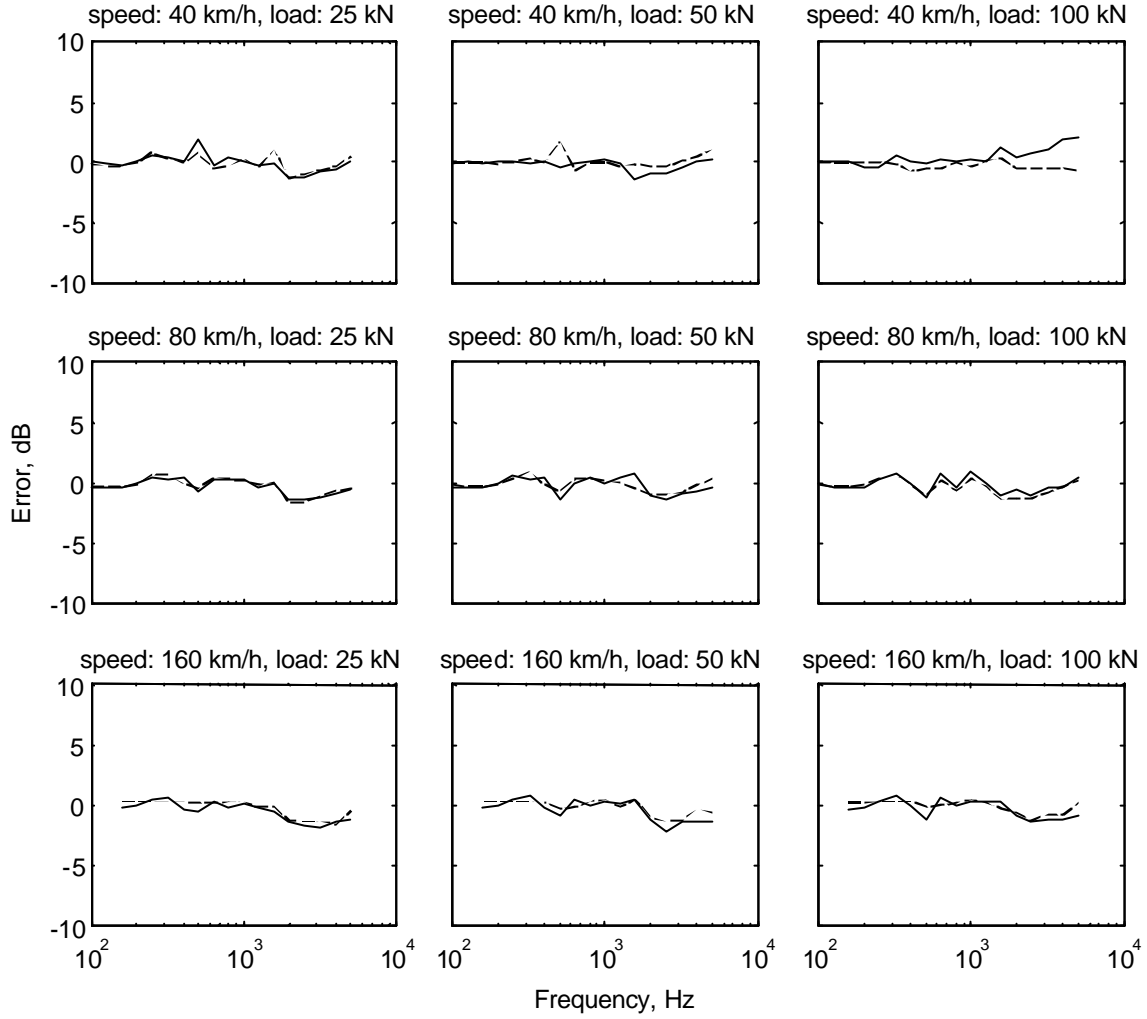
Figure 17. Difference between the wheel velocity of the simplified modal wheel obtained by the direct and hybrid methods (hybrid method based on the mass/spring model of Fig. 7). ¾¾ 2 mm new flat, - - - 1 mm new flat.

The corresponding errors introduced by the hybrid method based on a mass model for the wheel are shown in Figure 18. Taking the mean of the absolute value of the differences between the direct and indirect results, gives an average error of between 0.2 and 0.7 dB. These differences are not large, but sufficient to justify the use of the mass/spring model rather than a simple mass model.

Figure 18. Difference between the wheel velocity of the simplified modal wheel obtained by the direct and hybrid methods (hybrid method based on the unsprung mass only). ¾¾ 2 mm new flat, - - - 1 mm new flat.

6. APPLICATION TO NOISE FROM WHEEL FLATS

6.1 Impact force in the frequency-domain and equivalent roughness input

In this section the hybrid method introduced above will be used to calculate the noise radiated by a wheel and the track due to excitation by a wheel flat. The impact force is calculated in the time domain as in Section 4.3. Figure 12 showed the force spectra produced from new and rounded flats of depth 2 mm at four speeds.

Using equation (10) these force spectra can be converted to an equivalent roughness. This is performed at the discrete frequencies of the periodic force spectrum and the roughness spectrum is then converted to one-third octave form. The equivalent roughness spectra corresponding to the force spectra of Figure 12 are shown in Figure 19. Similar trends can be seen, since the same conversion is applied in each case.
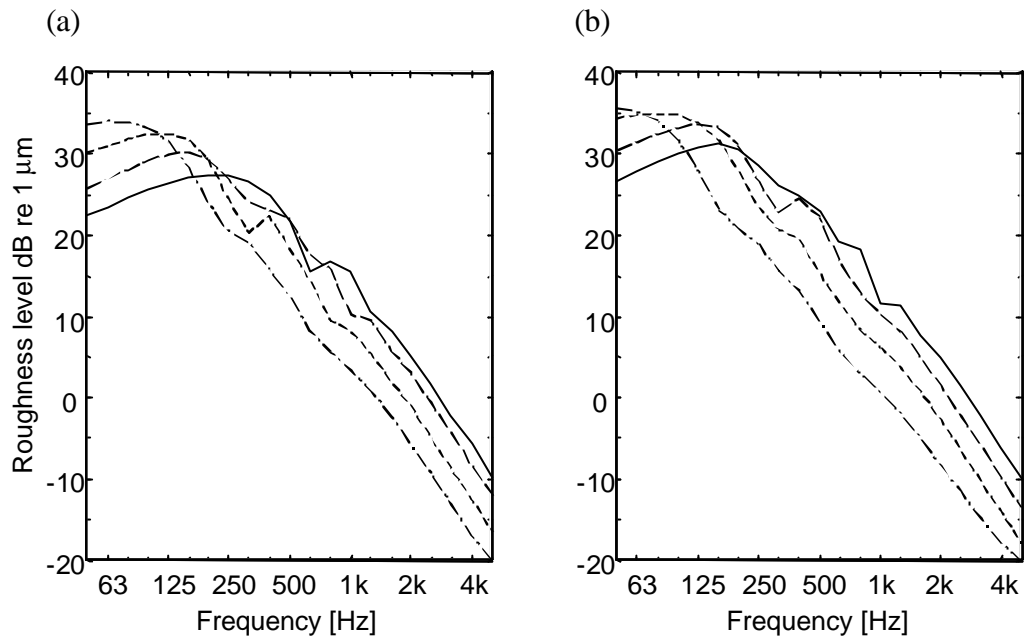
Figure 19. One-third octave spectra of the equivalent roughness due to wheel flats at different train speeds. (a) Due to 2 mm newly formed flats, (b) due to 2 mm rounded flats. ¾¾ At 120 km/h, - - - at 80 km/h, ✕✕✕at 50 km/h, - ✕- ✕at 30 km/h.
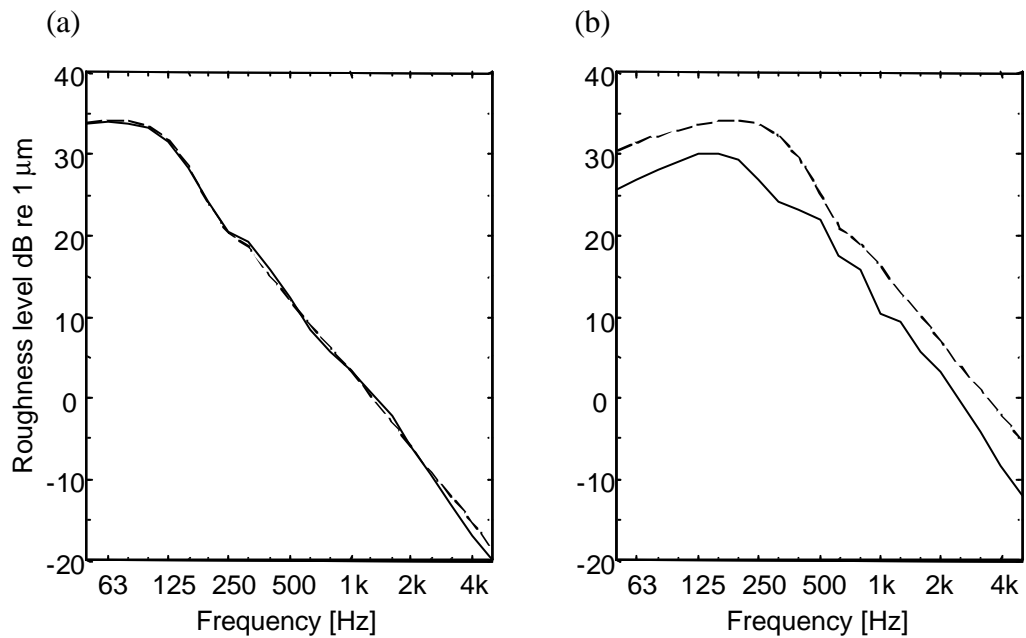

Figure 20. Comparison of one-third octave spectra of the equivalent roughness due to 2 mm newly formed flats with the original displacement input. (a) At 30 km/h, (b) at 80 km/h. ¾¾ Equivalent roughness excitation, - - - original displacement input.

In Figure 20 two of these curves are compared with the spectrum of the original relative displacement input used in each case, i.e. based on equation (4). At a speed of 30 km/h, the equivalent roughness spectrum is very similar to the spectrum of the original input, even though from Figure 11(a) it can be seen that loss of contact occurs momentarily and the maximum contact force is more than four times the nominal load of 100 kN. From this it is clear that, provided loss of contact does not occur, (i) the equivalent roughness can be taken directly from the wheel flat geometry, modified to allow for the curvature of the wheel, and (ii) the non-linear contact stiffness can be replaced by an equivalent linear spring. The latter conclusion has already been drawn in relation to random roughness inputs [9].

At 80 km/h, however, the equivalent roughness spectrum is about 3 – 5 dB lower than the spectrum of the original input. Figure 11(b) shows that contact is lost twice during the wheel flat event for a period of between 1 and 2 ms. The first loss of contact occurs during the maximum part of the input irregularity. This means that this part of the irregularity does not excite the wheel/rail system; the shape of the irregularity during loss of contact is actually arbitrary and therefore does not contribute to the excitation.

6.2 Impact noise due to wheel flats

The equivalent roughness spectra derived in the previous section are now used as inputs to a frequency-domain calculation of wheel/rail noise. For this the TWINS model[6, 7] is used. The wheel is represented by its full modal basis in the frequency range up to 6 kHz, determined from a finite element model. The track is modelled by a Timoshenko beam continuously supported on layers of damped springs and mass (see Figure 6). Track parameters are listed in Table 1. Wheel/rail interaction is included in both vertical and lateral directions, the excitation being in the vertical direction.

Figures 21 and 22 show predicted overall sound power radiated by one wheel and the associated track vibration. Results are shown for new and rounded flats, of 1 mm and 2 mm depth and at various speeds. As the speed increases, the noise at frequencies above about 200 – 400 Hz increases. Generally the noise from the 2 mm flats is greater than that from the 1 mm flats, and the new flats produce slightly more noise than the rounded flats for a given depth.
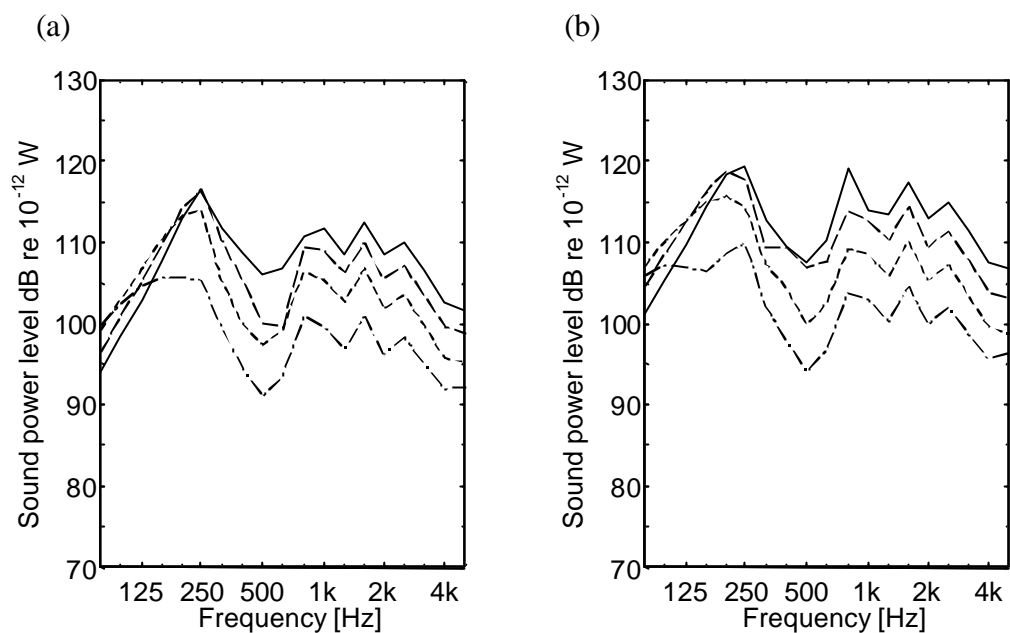
Figure 21. Sound power level due to wheel and track from a rounded wheel flat. (a) 1 mm flat, (b) 2 mm flat. - ×- ×30 km/h, ✕✕✕50 km/h, - - - 80 km/h, ¾¾ 120 km/h.
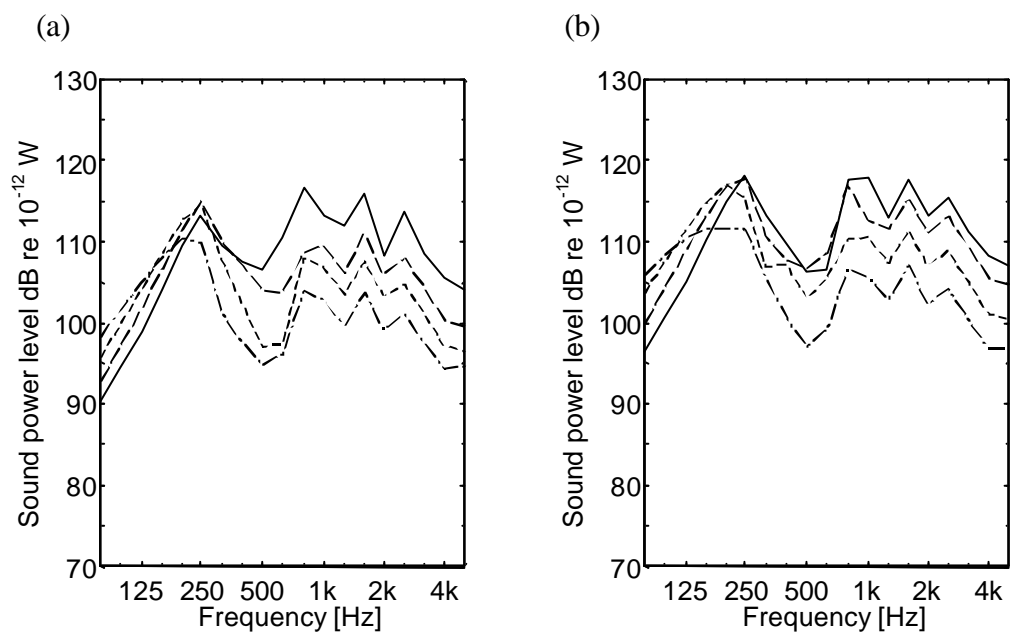

Figure 22. Sound power level due to wheel and track from a new wheel flat. (a) 1 mm flat, (b) 2 mm flat. - ×- ×30 km/h, ✕✕✕50 km/h, - - - 80 km/h, ¾¾ 120 km/h.

These results may be compared with Figure 23 which shows the sound power predicted for the same wheel/track combination from typical roughness spectra. In the left-hand figure the roughness represents cast-iron tread-braked vehicles on good quality track. In Figure 23(b) the noise is predicted for a corrugated track roughness spectrum. For the wheel flats that have been considered, the noise generated exceeds that due to the tread-braked wheel roughness at all

−27−

speeds and in all frequency bands, although the noise due to roughness increases more rapidly with speed so that at sufficiently higher speeds it can be expected to dominate. For corrugated track, the noise due to roughness exceeds that due to wheel flats at 120 km/h.
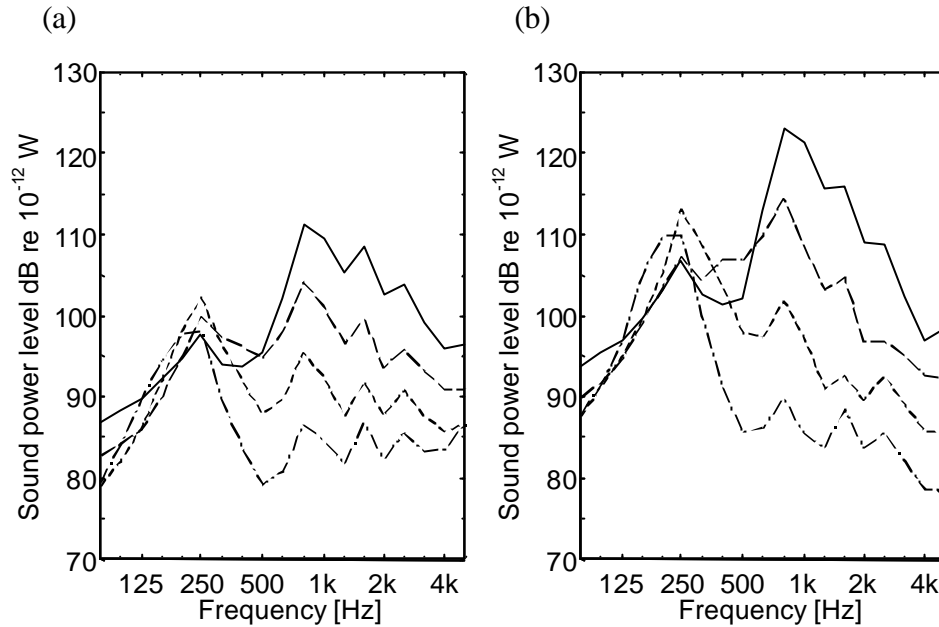

Figure 23. Sound power level due to wheel and track from the roughness (a) on a typical tread-braked wheel, (b) on corrugated track. - ×- ×30 km/h, ✺✺✺50 km/h, - - - 80 km/h, ¾¾ 120 km/h.
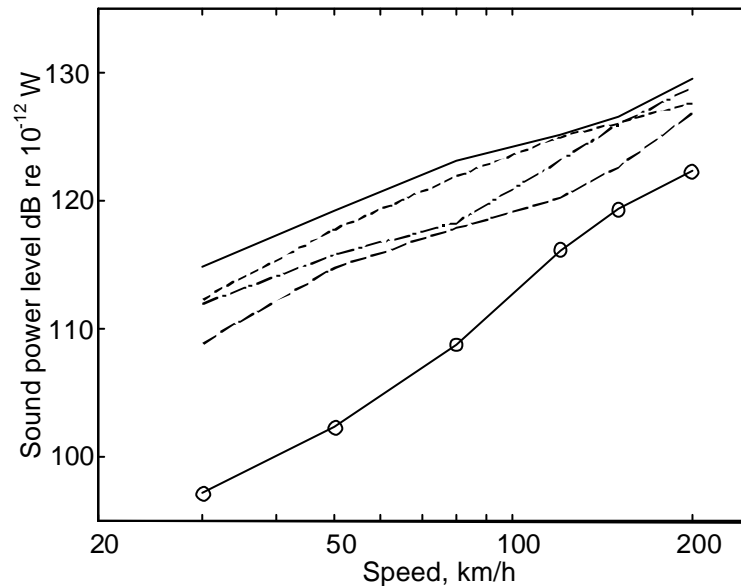

Figure 24. Sound power radiated by one wheel and the associated track vibration. - - - 1 mm rounded flat, ✺✺✺2 mm rounded flat, - ×- ×1 mm new flat, - - - - 2 mm new flat, o- - -o rolling noise due to roughness (tread-braked wheel).

Figure 24 shows a summary of the variation of the overall A-weighted sound power level with train speed. The predicted noise level due to roughness excitation increases at a rate of approximately $30 \log_{10} V$, where V is the train speed, whereas the noise due to flats increases at an average of around $20 \log_{10} V$. This variation with speed indicates that the radiated sound due to wheel flats continues to increase with increasing speed, even though loss of contact is occurring. For example, loss of contact is found to occur for the newly formed 2 mm flat at speeds above 30 km/h and for the rounded 2 mm flat above 50 km/h.

Below these speeds, Figure 20 showed that the equivalent roughness closely follows the original relative displacement input. Figure 25 shows the impact noise predicted from the original relative displacement input for a range of speeds. Compared to the equivalent roughness, this gives a higher noise level once loss of contact occurs and its slope is close to $30 \log_{10} V$. For lower speeds, although not predicted, the $30 \log_{10} V$ curves can be expected to apply. According to Vér et al [4] the noise was expected to reach a constant level when loss of contact occurs. The results here, however, which are based on a more comprehensive model, do not support this. Above the critical speed of Vér et al, a change occurs in the slope of noise level with speed, but a constant level is not reached.
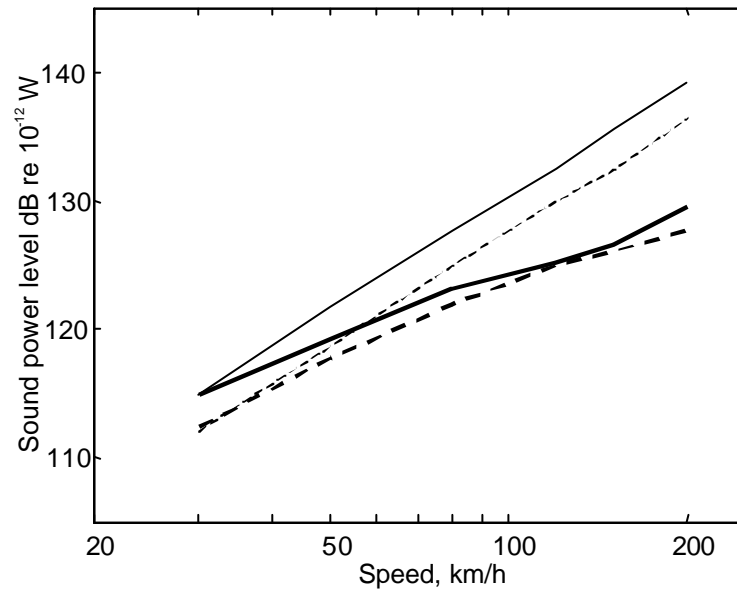

Figure 25. Sound power radiated by one wheel and the associated track vibration due to flats. ▨▨▨2 mm rounded flat, - - - 2 mm new flat. Thick lines: from equivalent roughness, thin lines from original relative displacement input.

All the results presented so far in this section have been for a wheel load of 100 kN. For lower wheel loads, the likelihood of loss of contact is increased [9]. At low speeds, where

contact is not lost, the equivalent roughness will closely follow the spectrum of the displacement input (Figure 20) and so the results for different wheel loads will be similar. At higher speeds, greater loss of contact will occur for lower wheel loads and therefore the noise level will be lower.

Figure 26 shows the overall A-weighted sound power level plotted against train speed for a 2 mm rounded flat at three values of wheel load. The corresponding TWINS calculations include the effect of the change in the contact stiffness. For 25 and 50 kN loads, loss of contact occurs for all speeds considered, whereas for 100 kN it only occurs at 50 km/h and above. For most of the results shown here, therefore, the noise level reduces as the wheel load is reduced. For a halving of the wheel load, the noise level due to the flat is reduced by about 3 dB. This corresponds to the difference between typical passenger vehicles (50 kN) and loaded freight vehicles (100 kN). In contrast, rolling noise due to roughness is relatively insensitive to variations in the wheel load, changing by only 0.7 dB between 50 and 100 kN due to a change in contact stiffness[2].
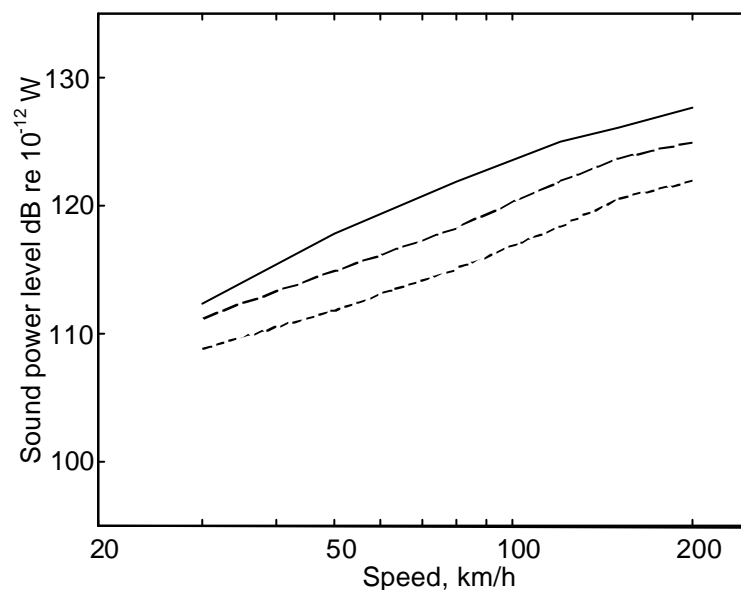

Figure 26. Sound power radiated by one wheel and the associated track vibration for a 2 mm rounded flat. - - - - for 100 kN wheel load, - - - for 50 kN wheel load, ▨▨▨for 25 kN wheel load.

---

[2] This ignores the additional effect of wheel load on the contact patch length and hence the filtering of the roughness.

7. FURTHER WORK

The model developed in this study requires validation by comparison of its results with measurements. The 1/5 scale model rig available at ISVR should be used to validate the parametric dependencies predicted by the model such as the dependence on speed, preload and flat size and shape. In this case, due to the experimental arrangement, it would be preferable to measure the vibration of the wheel and rail rather than noise. Validation should also be carried out at full scale. This would require measurements of the noise due to a wheel flat of known dimensions at different speeds, for example by means of a microphone mounted under a vehicle. This would allow the predicted $20 \log_{10} V$ dependence to be verified.

Apparatus is required for measuring the size and shape of actual wheel flats. The same apparatus could possibly be designed for use both on the scale rig and in the field on full scale wheels. Measurements could then be obtained of the actual shapes of wheel flats, which are expected to differ from the idealised shapes considered in this study. Using a numerical procedure, the relative displacement input from such flats can then be determined and calculations performed to compare the noise levels with those from the idealised flats.

Once the model has been validated in this way, it can be used to assess the noise levels from different sizes of wheel flat. A particular question that is worth answering is what length of flat gives a noise level that just exceeds that from roughness. This will depend on the speed, preload, initial roughness, and the shape of the flat.

Finally, it should be noted that the model presented here does not include any consideration of the finite size of the contact zone, other than via the contact stiffness. Thus the wheel and rail are considered to be connected at a point. The non-zero contact area may have the effect of attenuating high frequency components of the excitation, as is found for roughness excitation [12]. In order to allow for this effect, which will vary according to the contact force or deflection, a numerical procedure could be adopted, based on the Distributed Point Reacting Springs (DPRS) model of Remington and Webb [13], with inclusion of the wheel and rail dynamic models introduced in this study.

8. CONCLUSIONS

A numerical model has been developed to predict the wheel/rail dynamic interaction due to wheel-flat excitation. The form of the relative displacement excitation between the wheel and rail differs from the profile of the wheel flat due to the finite curvature of the wheel. To allow for the non-linear contact spring, and the possibility of loss of contact between the wheel and the rail, a time-domain model is required. This uses simplified dynamic models of the wheel and the track and a non-linear model of the contact spring between them. Results have been compared with published measurement data and shown to be in good agreement. For a newly formed wheel flat, of depth 2 mm and length 86 mm, loss of contact is found to occur for speeds above 30 km/h. For a rounded flat of the same depth but overall length 121 mm the speed at which loss of contact first occurs increases to about 50 km/h. At higher speeds a second loss of contact occurs after the initial impact.

In order to predict the consequent noise radiation, the wheel/rail interaction force is transformed into the frequency domain, and then converted back to an equivalent roughness spectrum. This spectrum is used as the excitation to a linear, frequency-domain model of wheel/rail interaction to predict the noise. This hybrid approach has been shown to be adequate by comparing direct and hybrid calculations for a wheel with a single, lightly-damped resonance.

As the train speed increases, the force spectrum and consequently the noise radiation, contains greater amplitudes at high frequencies and the overall noise level due to wheel flat excitation increases with the train speed V at a rate of roughly $20 \log_{10} V$ once loss of contact occurs. This differs from rolling noise due to roughness excitation which generally increases at $30 \log_{10} V$. The noise from flats of depth 1 mm and 2 mm exceeds that due to typical roughness on tread-braked wheels and good quality track for all speeds up to at least 200 km/h. The results do not show a critical speed above which the level remains constant, as suggested by Vér et al [4]. As the wheel load increases, the noise from wheel flats increases. The difference between a load of 50 kN, typical of passenger stock, and 100 kN, typical of loaded freight vehicles, is about 3 dB. In contrast, the rolling noise due to roughness is relatively insensitive to wheel load.

ACKNOWLEDGEMENTS

REFERENCES

1   J. JERGÉUS 1998 Railway wheel flats - martensite formation, residual stresses and crack propagation. PhD thesis, Chalmers University of Technology, Gothenburg, Sweden.

2   S. G. NEWTON and R. A. CLARK 1979 An investigation into the dynamic effects on the track of wheelflats on railway vehicles. *Journal of Mechanical Engineering Science* **21,** 287–297.

3   Joint Committee on Relation between Track and Equipment of the Mechanical and Engineering Divisions, AAR 1952 Effect of flat wheels on track and equipment (abstract of report) American Railway Engineering Association **53**, 423–448.

4   I. L. VÉR, C. S. VENTRES and M. M. MYLES 1976 Wheel/rail noise—Part III: Impact noise generation by wheel and rail discontinuities. *Journal of Sound and Vibration* **46**, 395–417.

5   P. J. REMINGTON 1987 Wheel/rail squeal and impact noise: What do we know? What don't we know? Where do we go from here? *Journal of Sound and Vibration* **116**, 339–353.

6   D. J. THOMPSON and M. H. A. JANSSENS 1997 TWINS: Track-wheel interaction noise software. Theoretical manual (version 2.4), TNO report TPD-HAG-RPT-93-0214, TNO Institute of Applied Physics, Delft.

7   D.J. THOMPSON, B. HEMSWORTH and N. VINCENT 1996 Experimental validation of the TWINS prediction program for rolling noise, part 1: description of the model and method. *Journal of Sound and Vibration* **193**, 123-135.

8   S. L. GRASSIE, R. W. GREGORY, D. HARRISON and K. L. JOHNSON 1982 The dynamic response of railway track to high frequency vertical excitation. *Journal of Mechanical Engineering Science* **24**, 77–90.

9   T.X. WU and D.J. THOMPSON 2000 Theoretical investigation of wheel/rail non-linear interaction due to roughness excitation. ISVR Technical Memorandum No. 852.

10 D.J. THOMPSON and C.J.C. JONES 2000 A review of the modelling of wheel/rail noise generation. *Journal of Sound and Vibration* **231**, 519-536.

11 D.J. THOMPSON 1993 Wheel-rail noise generation, part V: inclusion of wheel rotation. *Journal of Sound and Vibration* **161**, 467-482.

12 D.J. THOMPSON 1996 On the relationship between wheel and rail surface roughness and rolling noise. *Journal of Sound and Vibration* **193**, 149-160.

13 P. J. REMINGTON and J. WEBB 1996 Estimation of wheel/rail interaction forces in the contact area due to roughness. *Journal of Sound and Vibration* **193**, 83-102.

Appendix A. Wheel centre trajectory for a rounded flat

Consider a wheel profile consisting of a flat of depth d, with on either side a smooth transition defined by a quadratic function. This is shown schematically in Figure A.1.
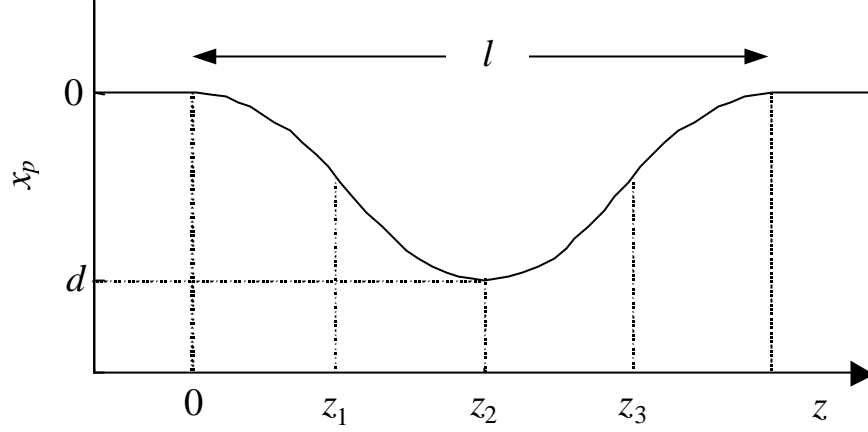

Figure A.1 Idealised 'rounded flat' profile

The wheel profile depth (positive downwards) can be written as

$$x_p(z) = \begin{cases} az^2, & 0 \le z \le z_1, \\ d - \dfrac{1}{2r}(z - z_2)^2, & z_1 \le z \le z_2, \end{cases} \tag{A1}$$

where $z = z_2 = l/2$ is the point at the centre of the flat, $z = z_1$ is the point at which the two curves meet, and a is a constant determining the extent of the transition. For $z < 0$, $x_p = 0$, while for $z > z_2$, $x_p(z) = x_p(2z_2 - z)$.

At $z = z_1$ it is required that x_p and its first derivative are continuous. This gives two equations relating a, z_1 and z_2:

$$2az_1 = \frac{(z_2 - z_1)}{r} \tag{A2}$$

$$az_1^2 = d - \frac{(z_2 - z_1)^2}{2r} \tag{A3}$$

These can be rearranged to give:

$$z_1 = \frac{z_2}{2ar + 1} \tag{A4}$$

$$d = az_1{}^2(2ar+1) = \frac{az_2{}^2}{2ar+1} \tag{A5}$$

Suppose that this profile is actually on the rail surface rather than on the wheel. Then, as a round wheel rolls over it, the wheel and the rail profile share a common tangent, see Figure A.2.
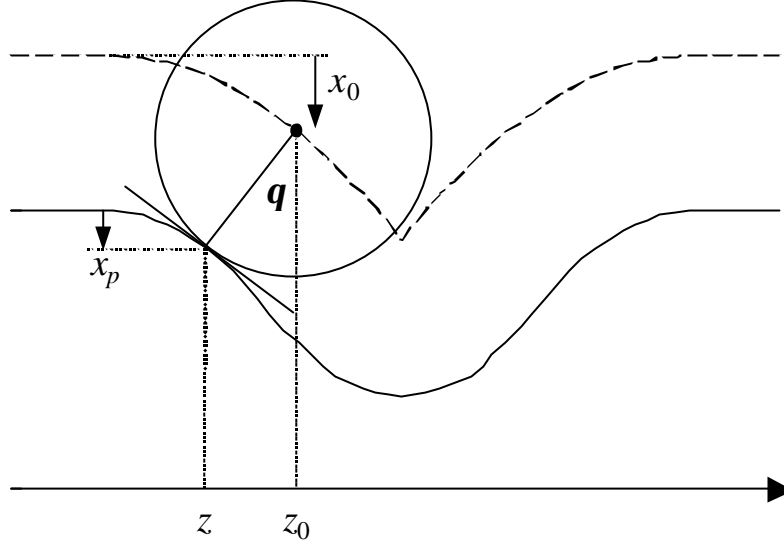

Figure A.2 Rolling of a wheel on an idealised 'rounded flat' profile

When the contact is at z, the gradient is

$$q \approx \tan q = x'_p(z) = 2az , \tag{A6}$$

and the wheel centre is located at

$$z_0 = z + r\sin q \approx z(1+2ar). \tag{A7}$$

Note from equations (A4) and (A7) that when $z = z_1$, $z_w = z_2$, at which point the contact jumps to z_3. The height of the wheel centre is thus given by

$$x_0(z_0) = x_r(z) + r(1-\cos q) \approx az^2 + r\frac{q^2}{2} ,$$

$$x_0(z_0) \approx az^2(1+2ar) . \tag{A8}$$

Rewriting this in terms of z_0 (from equation (A7)),

$$x_0(z_0) \approx \frac{az_0{}^2}{(1+2ar)} , \tag{A9}$$

and, from equation (A5), the wheel centre trajectory can be written as

$$x_0(z_0) = d\frac{z_0{}^2}{z_2{}^2} = 4d\frac{z_0{}^2}{l^2} \quad 0 \le z_0 \le l/2. \tag{A10}$$

By symmetry, $x_0(z_0) = x_0(l - z_0)$ for $l/2 \le z_0 \le l$.

Appendix B. Results of calculations showing that the interaction force depends on the wheel receptance

A finite element model of a 920 mm diameter standard freight wheel is used. The receptance of this wheel is compared in Figure B1 with that of the track and of the contact spring. The track corresponds to the parameters in Table 1 and the contact spring has the linearised stiffness of 1.14×10^9 N/m, corresponding to a load of 50 kN. Also shown is the receptance of the wheel represented using the mass/spring model shown in Figure 7.

In Figure B2 the contact force per unit roughness is shown. This is predicted from the linear model with interaction only in the vertical direction, *i.e.* using equation (9). Sharp dips can be seen in the force spectrum at high frequencies corresponding to each wheel resonance. For the mass and mass/spring models of the wheel the contact force is similar to that predicted from the full wheel model below 1 kHz, whilst at high frequencies they both show a result part way between the peaks and troughs of the full model.

From these force spectra, the wheel response at the contact zone is found by multiplying the force by the wheel receptance. This is shown in Figure B3. Although broad peaks can be seen that correspond to each resonance at high frequency, these have a lower amplitude and broader bandwidth consistent than the free wheel receptance (Figure B1). For the single mass model of the wheel the response is much lower at high frequency.

The wheel vertical response is also shown in the form of one-third octave band spectra in Figure B4. This also compares the result of predicting the response of the detailed wheel model for coupling only in the vertical direction with that obtained when coupling in the vertical and lateral directions is taken into account. The differences between these two simulations are small.

Figures B5 and B6 show two examples of one-third octave band responses obtained when the contact force and wheel receptance are incorrectly matched. In Figure B5 results are shown for the nominal wheel and for a variant of this wheel in which all the natural frequencies have been increased by 5%. In one-third octave form these two results are similar. However, the third curve shows the result of combining the force spectrum for the original wheel with the receptance of the modified wheel. In this case the peaks in the receptance and the dips in the force spectrum do not align and the predicted response at high frequencies is 10 to 20 dB too high.

Similar results are shown in Figure B6. Here the response of the nominal wheel is compared with the response calculated for this wheel using the force derived from the simple mass/spring model of Figure 7. Also shown is the response for the nominal wheel calculated with the correct force spectrum but with the calculation performed in one-third octave bands. In both these cases the response is again too large at high frequencies.
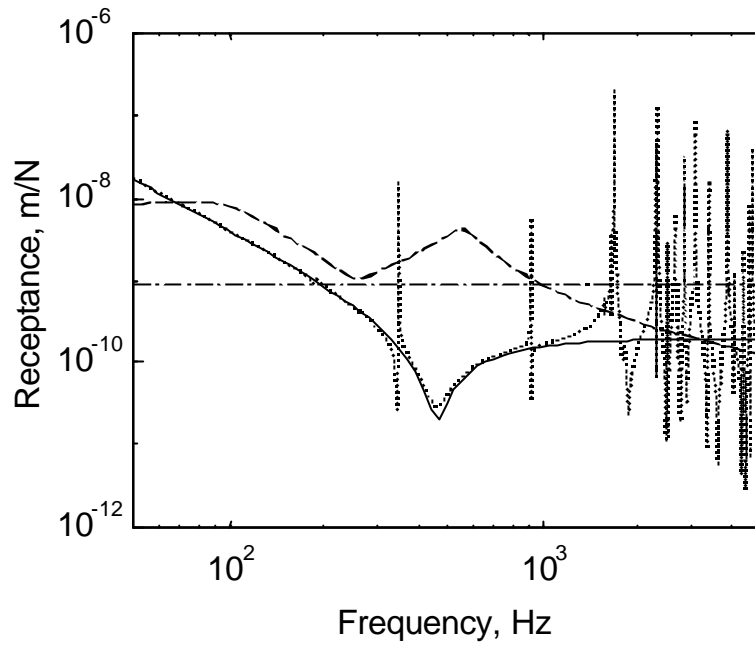
Figure B1. Receptance of the wheel modelled using finite elements (✕✕✕✕) and using the model of Fig. 7 (- - - -), receptance of rail (- - -) and receptance of contact spring (- ✕- ✕).

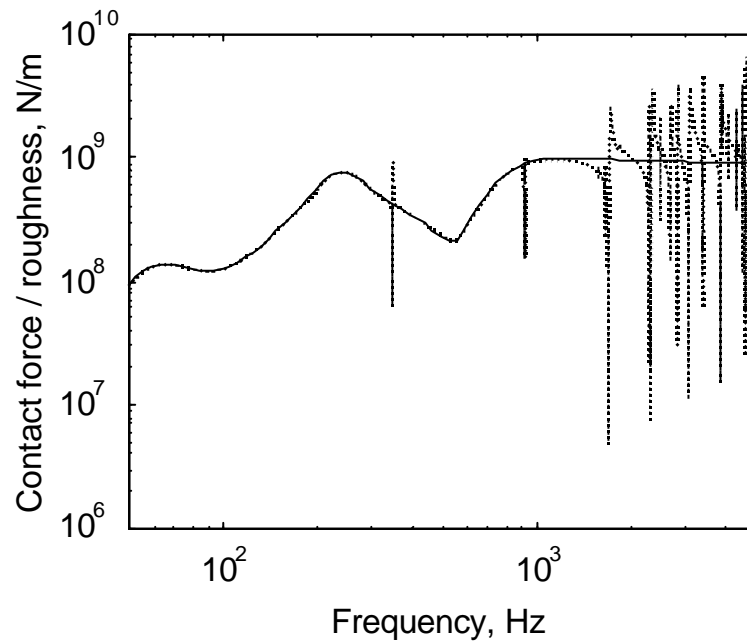*Figure B2. Contact force for unit roughness amplitude for the wheel modelled using finite elements (✕✕✕✕) and using the model of Fig. 7 (- - - -).*
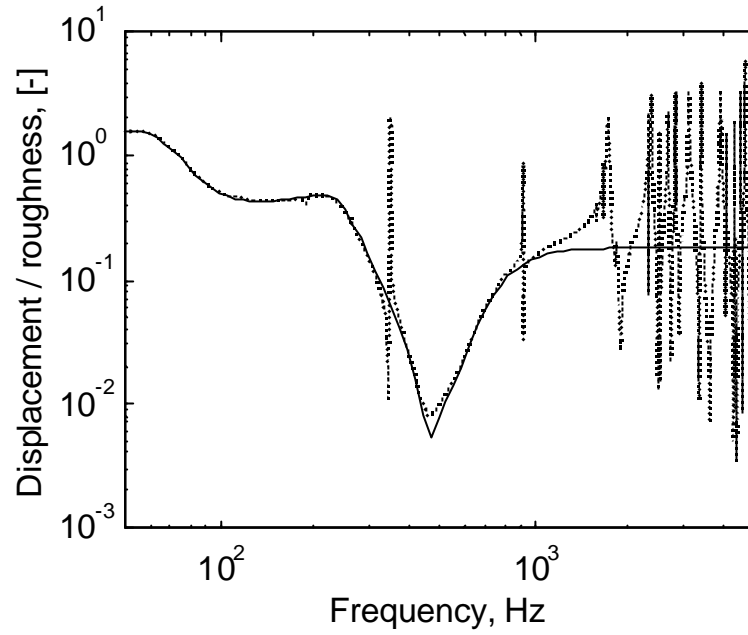
Figure B3. Vibration of wheel at contact point expressed as displacement for unit roughness amplitude, for the wheel modelled using finite elements (⨉⨉⨉⨉) and using the model of Fig. 7 (- - - -).
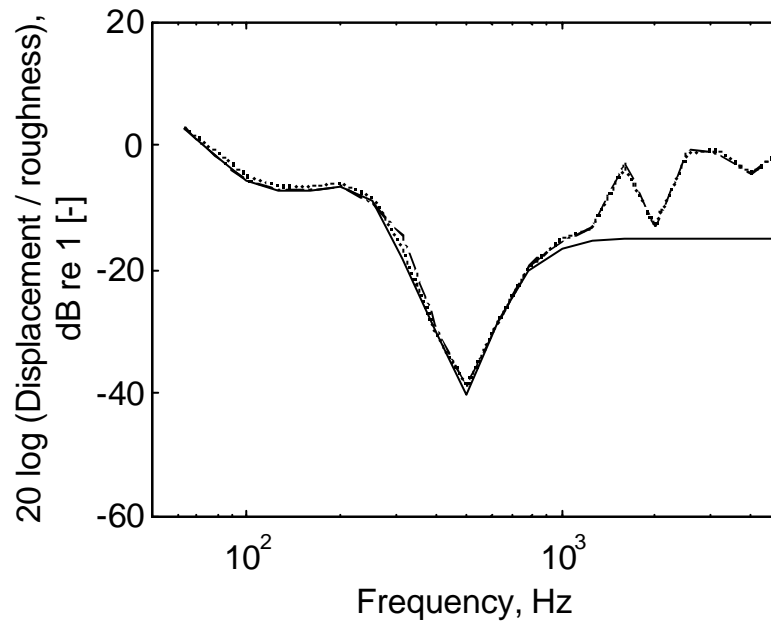

Figure B4. Vibration of wheel at contact point expressed as displacement for unit roughness amplitude in one-third octave bands. ⨉⨉⨉⨉for the wheel modelled using finite elements, - ×- ×ditto including wheel/rail coupling in two directions, - - - - using the model of Fig. 7.
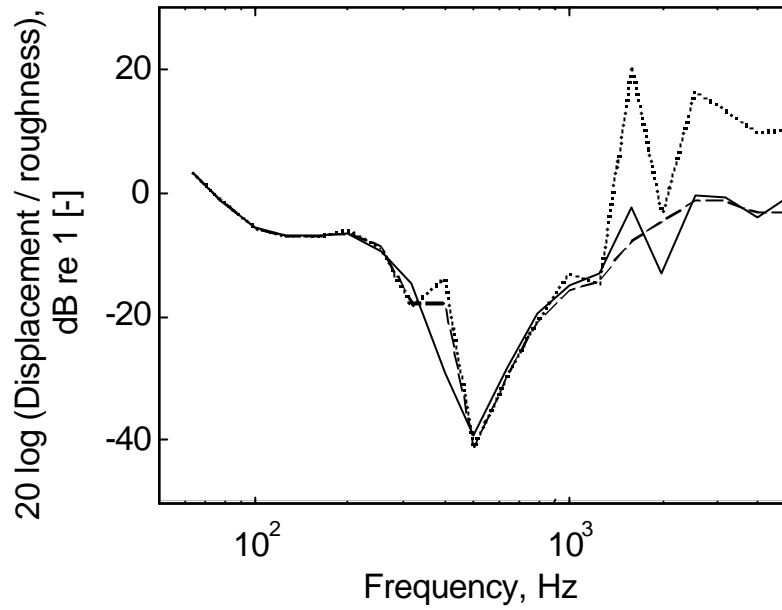
Figure B5. Vibration of wheel at contact point expressed as displacement for unit roughness amplitude in one-third octave bands, predicted from finite element wheel model. - - - - nominal wheel, - - - wheel with natural frequencies shifted by 5%, ✳✳✳force spectrum for nominal wheel times receptance of modified wheel.
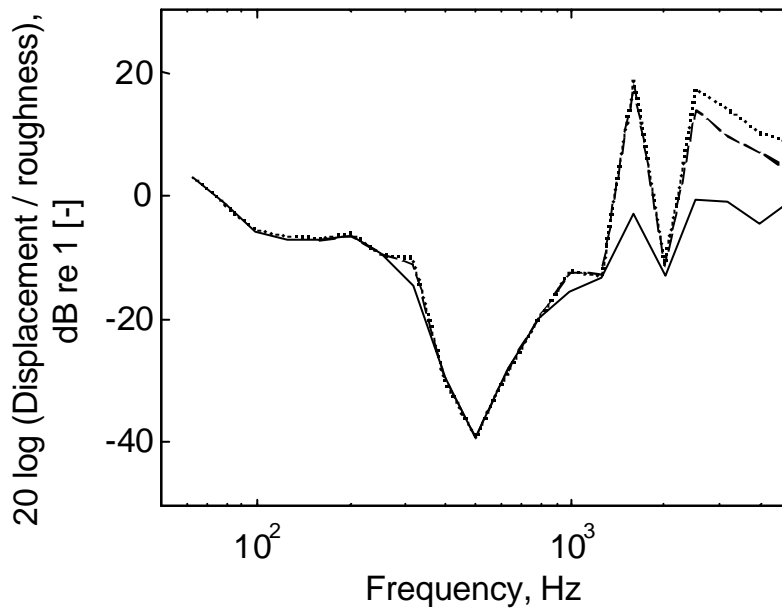

Figure B6. Vibration of wheel at contact point expressed as displacement for unit roughness amplitude in one-third octave bands, predicted from finite element wheel model. - - - - nominal wheel, - - - force spectrum for mass/spring wheel of Fig. 7 times receptance of nominal wheel, ✳✳✳force spectrum for nominal wheel times wheel receptance in one-third octave bands.